WSRC-TR-2007-00439, REVISION 0

Keywords: **Hydrogen Kinetics,**
Hydrogen Storage Vessel
Metal Hydride

Retention: Permanent

Geometry, Heat Removal and Kinetics Scoping Models for Hydrogen Storage Systems

Bruce J. Hardy

November 16, 2007

Washington Savannah River Company
Savannah River Site
Aiken, SC 29808

Prepared for the U.S. Department of Energy
Under Contract Number DEAC09-96-SR18500

SRNL
SAVANNAH RIVER NATIONAL LABORATORY

Printed in the United States of America

Prepared For the
U.S. Department of Energy

WSRC-TR-2007-00439, REVISION 0

Keywords: **Hydrogen Kinetics,**
Hydrogen Storage Vessel
Metal Hydride

Retention: Permanent

Geometry, Heat Removal and Kinetics Scoping Models for Hydrogen Storage Systems

Bruce J. Hardy

November 16, 2007

Washington Savannah River Company
Savannah River Site
Aiken, SC 29808

Prepared for the U.S. Department of Energy Under Contract Number DEAC09-96-SR18500

SRNL
SAVANNAH RIVER NATIONAL LABORATORY

TABLE OF CONTENTS

LIST OF FIGURES

LIST OF TABLES

LIST OF ACRONYMS

DOE	Department of Energy
UTRC	United Technologies Research Center®

NOMENCLATURE

A = Surface area [m^2]

C = Concentration of H_2 [mol H_2/m^3 of interparticle void]

C_{eqv} = Equivalent concentration of $NaAlH_4$ [moles/m^3] based on the initial concentrations of all metal species

= $C_{10} + 3C_{20} + C_{30}$

C_{NaH} = The bulk concentration of NaH [mol NaH/m^3]

C_{NaAlH_4} = The bulk concentration of $NaAlH_4$ [mol $NaAlH_4/m^3$]

C_{nd} = The non-dimensionalized concentration of $H_2 = \frac{C}{C_{ref}}$

C_p = Specific heat of coolant [J/(kg- K)]

$C_{p_{metal}}$ = Specific heat of the metal [J/(kg-K)]

C_1 = Concentration of $NaAlH_4$ [moles/m^3]

C_2 = Concentration of Na_3AlH_6 [moles/m^3]

C_3 = Concentration of NaH [moles/m^3]

$C_{1\,0}$ = Initial concentration of $NaAlH_4$ [moles/m^3]

$C_{2\,0}$ = Initial concentration of Na_3AlH_6 [moles/m^3]

$C_{3\,0}$ = Initial concentration of NaH [moles/m^3]

D = Inner diameter of coolant tube [m]

D_{cool} = Inner diameter of coolant tube [m]

D_p = Mean diameter of particles in bed [m]

D_{H_2} = Diameter hydrogen feed tube [m]

D_{cool_outer} = Outer diameter of coolant tube, including sleeve formed by extrusion of fin [m].

f = Friction factor

G = Mass flux [kg/m^2-s]

G_{H_2} = Hydrogen gravimetric density [(Mass H2)/(Mass NaAlH4 From NaH)]

$\vec{g}$ = Gravitational acceleration vector [m/s^2]

h = Specific enthalpy [J/kg]

$h_{conv\ cool}$ = Convection heat transfer coefficient for heat transfer fluid [W/m^2- K]

h_f = Convection heat transfer coefficient for the heat transfer fluid [W/(m^2- K)]

$h_{H2\ cool}$ = Convection heat transfer coefficient for H_2 in the feed tube [W/m^2- K]

ι = Specific internal energy [J/kg]

k = Thermal conductivity of the metal hydride bed [W/(m-K)]

k_f = Thermal conductivity of the heat transfer fluid [W/(m- K)]

k_{metal} = Thermal conductivity of the metal [W/(m-s)].

L = Characteristic length [m].

m_{H_2} = Mass of recoverable hydrogen sorbed in the bed [kg]

m_{system} = Total mass of loaded storage tank, including the bed loaded with H_2, fins, liner gaps and pressure vessel. The mass of the heat transfer fluid is not included.

P = Pressure [Pa]

M_i = Molecular weight of species i per mole [kg/g-mole]

M_{H_2} = Gram molecular weight of H_2 [kg/g-mol] = 0.002016 kg/g-mole

M_{NaH} = Gram molecular weight of NaH [kg/g-mol]

M_{NaAlH_4} = Gram molecular weight of $NaAlH_4$ [kg/g-mol] = 0.054 kg/g-mole

$M_{Na_3AlH_6}$ = Gram molecular weight of Na_3AlH_6

$\hat{n}$ = Outward normal to surface

n_{NaH} = Number of moles of NaH

n_{NaAlH_4} = Number of moles of $NaAlH_4$

$n_{Na_3AlH_6}$ = Number of moles of Na_3AlH_6

n_{H_2} = Total number hydrogen feed tubes

$Nu_D = \frac{hD}{k}$ = Nusselt number based on diameter, D

P = Pressure [Pa]

$P_{nd} = \frac{P}{P_{ref}}$ = Non-dimensional pressure

P_{ref} = Reference pressure [Pa]

$Pr = \frac{\nu}{\alpha}$ = Prandtl number

$\vec{q}''$ = Heat flux vector [W/m^2]

q'' = Heat flux [W/m^2]

R = Gas constant

$Re_D = \frac{GD}{\mu}$ = Reynolds number based on diameter, D

S = Arc length [m]

S_{H_2} = Rate of H_2 generation per volume of bed from all chemical reactions [mol $H_2/(m^3$ - s)],

$S_{H_2} > 0$ if H_2 is produced

$S_{H_2} < 0$ if H_2 is removed

S_1 = The arc length of tubes in contact with coolant, lying within area A_1 [m]

S_2 = The arc length of tubes in contact with coolant, lying within area A_2 [m]

$T_{coolant\ bulk}$ = Bulk temperature of the heat transfer fluid [K]

$T_{nd} = \frac{T}{T_{ref}}$ = Non-dimensional temperature

$T_{H2\ bulk}$ = Bulk temperature of the H_2 in the feed tube [K]

T_{ref} = Reference temperature [K]

T_{wall} = Tube wall temperature [K]

V = Volume [m^3]

V_{system} = Total volume of storage tank, including the bed, fins, liner gaps and pressure vessel [m^3].

$\vec{v}$ = H_2 velocity [m/s]

u = x component of the velocity, $\vec{v}$ [m/s]

$u_{nd} = \frac{u}{U_{ref}}$ = Non-dimensional x-component of velocity

U_{ref} = Reference velocity [m/s]

v = y component of the velocity, $\vec{v}$ [m/s]

$v_{nd} = \frac{v}{U_{ref}}$ = Non-dimensional y-component of velocity

V_{system} = Total volume of storage tank, including the bed, fins, liner gaps and pressure vessel [m^3]

w = z component of the velocity, $\vec{v}$ [m/s]

$w_{nd} = \frac{w}{U_{ref}}$ = Non-dimensional z-component of velocity

Greek

α = Thermal diffusivity of coolant [m^2/s].

ΔC_{H_2} = Change in the concentration of H_2 [mole/m^3]

ΔC_{NaAlH_4} = Change in the concentration of $NaAlH_4$ [mole/m^3]

ΔH_i = Enthalpy of reaction on a molar basis of species i [J/(mol of i)]

ΔH_{rx} = Overall heat of reaction for uptake of H_2 by the hydride [J/g-mol].

$\Delta H_{rxn\ 1}$ = Heat of per mole of H_2 consumed going to left for reaction 1

= -37 kJ/(mol H_2)

$\Delta H_{rxn\ 2}$ = Heat of per mole of H_2 consumed going to left for reaction 2

= -47 kJ/(mol H_2)

Δn_{H_2} = Number of moles of H_2 consumed in going form NaH to $NaAlH_4$ [mole]

Δn_{NaAlH_4} = Number of moles of $NaAlH_4$ produced from NaH [mole]

ΔP = Pressure drop across the length of the tube [Pa]

ΔT = Change in bulk temperature of coolant over the heated length of the cooling tube [°C]

ε = Void between particles in bed

ν = Kinematic viscosity of coolant [m^2/s]

ρ = Mass density [kg/m^3]
ρ_i = Mass density of species i [kg/m^3]
ρ_{metal} = Density of the metal [kg/m^3].
μ = Viscosity [Pa-s]
$\underline{\underline{\tau}}$ = Stress tensor, having components τ_{ij} [N/m^2]
τ = Time required for H_2 loading [s].

Symbols and Operators

$\left.\frac{\nu_{H_2}}{\nu_{NaH}}\right|_{Rxn2}$ = Ratio of the stoichiometric coefficient of H_2 to NaH in reaction 2 = 0.5

$\left.\frac{\nu_{H_2}}{\nu_{NaAlH_4}}\right|_{Rxn1}$ = Ratio of the stoichiometric coefficient of H_2 to $NaAlH_4$ in reaction 1 = 1

$()_{H_2}$ = For H_2 gas
$()_R$ = For solid phase reactants
$()_P$ = For solid phase products
$()_I$ = For inert (non-reacting) material, such as metal foam

1.0 EXECUTIVE SUMMARY

It is recognized that detailed models of proposed hydrogen storage systems are essential to gain insight into the complex processes occurring during the charging and discharging processes. Such insight is an invaluable asset for both assessing the viability of a particular system and/or for improving its design. The detailed models, however, require time to develop and run. Clearly, it is much more efficient to begin a modeling effort with a good system design and to progress from that point. To facilitate this approach, it is useful to have simplified models that can quickly estimate optimal loading and discharge kinetics, effective hydrogen capacities, system dimensions and heat removal requirements. Parameters obtained from these models can then be input to the detailed models to obtain an accurate assessment of system performance that includes more complete integration of the physical processes.

This report describes three scoping models that assess preliminary system design prior to invoking a more detailed finite element analysis. The three models address the kinetics, the scaling and heat removal parameters of the system, respectively. The kinetics model is used to evaluate the effect of temperature and hydrogen pressure on the loading and discharge kinetics. As part of the kinetics calculations, the model also determines the mass of stored hydrogen per mass of hydride (in a particular reference form). As such, the model can determine the optimal loading and discharge rates for a particular hydride and the maximum achievable loading (over an infinite period of time). The kinetics model developed with the Mathcad® solver, runs in a mater of seconds and can quickly be used to identify the optimal temperature and pressure for either the loading or discharge processes. The geometry scoping model is used to calculate the size of the system, the optimal placement of heat transfer elements, and the gravimetric and volumetric capacities for a particular geometric configuration and hydride. This scoping model is developed in Microsoft Excel® and inputs the mass of hydrogen to be stored, mass of stored hydrogen to mass of hydride (from the kinetics model), component densities, etc. The heat removal scoping model is used to calculate coolant flowrates, pressure drops and temperature increases over the length of the cooling channels. The model also calculates the convection heat transfer coefficient required to remove the heat of reaction associated with hydrogen uptake. The heat removal model inputs dimensions and the mass of hydrogen to be stored directly from the geometry scoping model. Additionally, the model inputs the heats of reaction, the thermal properties of the coolant and the time required to charge the bed.

2.0 INTRODUCTION

Detailed models for hydrogen storage systems provide essential information about flow and temperature distributions and the utilization of the bed. However, before constructing a detailed model it is necessary to know the geometry and dimensions of the system, along with its heat transfer requirements, which depend on the limiting reaction kinetics. This document describes scoping models that were developed to estimate system dimensions required to store a given mass of hydrogen, determine coolant flowrates and temperatures required to remove heat generated by uptake or discharge reactions, evaluate the reaction kinetics models and, within the context of these models, determine limiting bed loading rates.

The system of scoping models is general and can be applied to any storage material and bed configuration. In this document, the system of models are applied to $TiCl_3$ catalyzed $NaAlH_4$ storage media in a cylindrical shell and tube storage configuration that has axially spaced fins, that extend in the radial direction; similar to that in Figure 2.0-1. Additionally, the kinetics scoping model is applied to α-AlH_3.

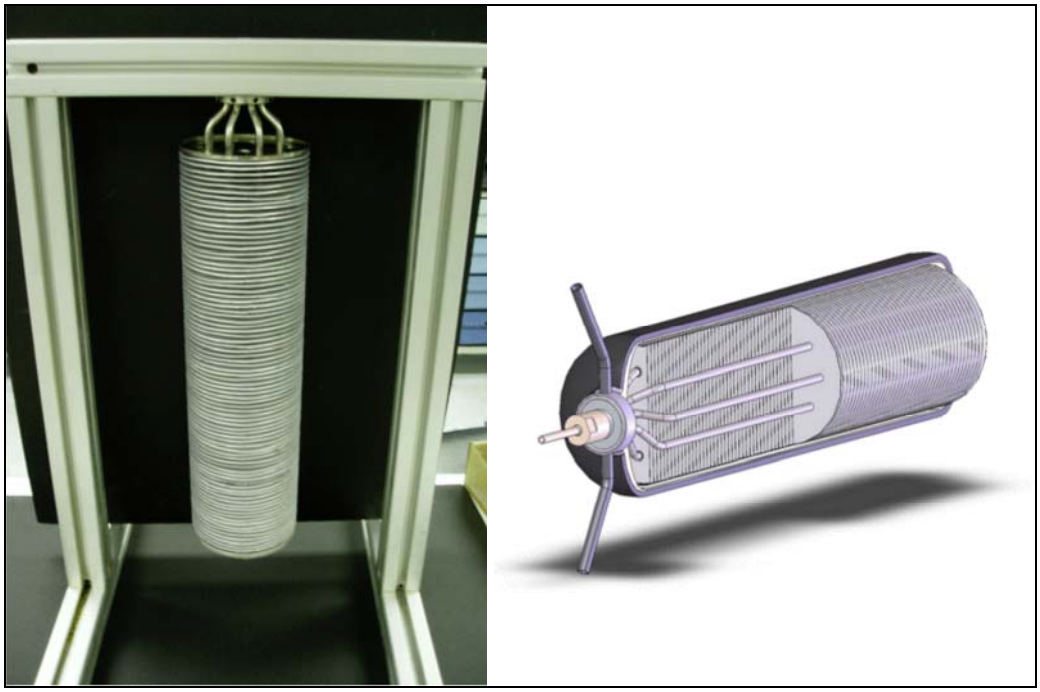

Figure 2.0-1 Illustration of a shell, tube and fin hydride bed configuration developed by the United Technologies Research Center™, East Hartford, Connecticut.

3.0 CHEMICAL KINETICS SCOPING MODEL

The effect of chemical kinetics on the hydrogen loading and discharge rates from a particular hydrogen storage material are evaluated using the chemical kinetics scoping

model, which is based on the Mathcad®, version 14.0.0.163, software. The model, which considers the dependence of reaction kinetics on temperature and pressure, is used to identify potential discrepancies in kinetics data, predict loading rates, and determine the gravimetric and volumetric capacities of the bed.

The equations governing reaction rates for hydrogen with the metal hydrides are dependent on the hydride and its reaction mechanism. In this document, the reactions for hydrogen uptake by $TiCl_3$ catalyzed sodium alanate, $NaAlH_4$, and by alpha aluminum hydride, α-AlH_3, are specifically addressed in Sections 3.1 and 3.2. The Mathcad® based model, however, may be applied to any metal hydride once its kinetics have been characterized.

3.1 Sodium Aluminum Hydride Reaction

The United Technologies Research Center™ (UTRC) developed an empirical kinetics model for hydrogen uptake and discharge reactions in $TiCl_3$ catalyzed $NaAlH_4$, see Attachments 3 and 4. The chemical balance equation for the reaction is

$$\underbrace{NaAlH_4}_{\text{Species 1}} \underbrace{\leftrightarrow}_{\text{Reaction 1}} \underbrace{\frac{1}{3}Na_3AlH_6}_{\text{Species 2}} + \frac{2}{3}Al + H_2 \underbrace{\leftrightarrow}_{\text{Reaction 2}} \underbrace{NaH}_{\text{Species 3}} + Al + \frac{3}{2}H_2 \qquad 3.1\text{-}1$$

To use the UTRC kinetics model, define the expressions:

$$\boxed{r_{1F} \equiv C_{eqv} A_{1F} \exp\left[-\frac{E_{1F}}{RT}\right]\left[\frac{P(C,T) - P_{eq1}(T)}{P_{eq1}(T)}\right]} \qquad 3.1\text{-}2a$$

$$r_{1B} \equiv -C_{eqv} A_{1B} \exp\left[-\frac{E_{1B}}{RT}\right]\left[\frac{P_{eq1}(T) - P(C,T)}{P_{eq1}(T)}\right] \qquad 3.1\text{-}2b$$

$$r_{2F} \equiv -C_{eqv} A_{2F} \exp\left[-\frac{E_{2F}}{RT}\right]\left[\frac{P(C,T) - P_{eq2}(T)}{P_{eq2}(T)}\right] \qquad 3.1\text{-}2c$$

$$r_{2B} \equiv C_{eqv} A_{2B} \exp\left[-\frac{E_{2B}}{RT}\right]\left[\frac{P_{eq2}(T) - P(C,T)}{P_{eq2}(T)}\right] \qquad 3.1\text{-}2d$$

where:
- r_{1F} = Hydriding (forward) reaction rate coefficient for reaction 1 [mole/(m^3 s)], see Eq. 3.1-1
- r_{1B} = Deydriding (backward) reaction rate coefficient for reaction 1 [mole/(m^3 s)], see Eq. 3.1-1
- r_{2F} = Hydriding (forward) reaction rate coefficient for reaction 2 [mole/(m^3 s)], see Eq. 3.1-1
- r_{2B} = Deydriding (backward) reaction rate coefficient for reaction 2 [mole/(m^3 s)], see Eq. 3.1-1
- C = Concentration of H_2 [mole/m^3]

C_{eqv} = Equivalent concentration of $NaAlH_4$ [mole/m^3] based on the initial concentrations of all metal species

= $C_{10} + 3C_{20} + C_{30}$

C_{10} = Initial concentration of $NaAlH_4$ [mole/m^3]

C_{20} = Initial concentration of Na_3AlH_6 [mole/m^3]

C_{30} = Initial concentration of NaH [mole/m^3]

$P_{eq1}(T)$ and $P_{eq2}(T)$ are the H_2 pressures, in Pa, in equilibrium with the $NaAlH_4$ and the Na_3AlH_6 metal hydrides, respectively, at temperature T, in [K]. These equilibrium pressures are given by the van't Hoff equations:

$$P_{eq1}(T) = 10^5 \exp\left[\frac{\Delta H_4}{RT} - \frac{\Delta S_4}{R}\right] \qquad 3.1\text{-}3a$$

$$P_{eq2}(T) = 10^5 \exp\left[\frac{\Delta H_2}{RT} - \frac{\Delta S_2}{R}\right] \qquad 3.1\text{-}3b$$

Values for the constants used in Eqs. 3.1-2a-d, and 3.1-3a-b are listed in Table 3.1-1

Table 3.1-1
Constants for the Rate and Equilibrium Expressions

Constant	Value
A_{1F}	10^8
A_{1B}	4×10^5
A_{2F}	1.5×10^5
A_{2B}	6×10^{12}
E_{1F}	80.0 kJ/mol
E_{1B}	110.0 kJ/mol
E_{2F}	70.0 kJ/mol
E_{2B}	110.0 kJ/mol
χ_{1F}	2.0
χ_{1B}	2.0
χ_{2F}	1.0
χ_{2B}	1.0
$\frac{\Delta H_1}{R}$	-4475
$\frac{\Delta S_1}{R}$	-14.83
$\frac{\Delta H_2}{R}$	-6150
$\frac{\Delta S_2}{R}$	-16.22

The reference for this model, contained in Attachment A-1, proposes the kinetics equations

$$\frac{dC_1}{dt} = \begin{cases} r_{1F}\left[\frac{3C_2(t)}{C_{eqv}} - C_{2sat}(T)\right]^{\chi_{1F}} & \text{if} \quad P \geq P_{eq1}(T) \\ r_{1B}\left[\frac{C_1(t)}{C_{eqv}}\right]^{\chi_{1B}} & \text{if} \quad P < P_{eq1}(T) \text{ and } C_1(t) \geq 0 \end{cases} \qquad 3.1\text{-}4a$$

and

$$\frac{dC_3}{dt} = \begin{cases} r_{2F}\left[\frac{C_3(t)}{C_{eqv}} - C_{3sat}(T)\right]^{\chi_{2F}} & \text{if} \quad P \geq P_{eq2}(T) \\ r_{2B}\left[\frac{3C_2(t)}{C_{eqv}}\right]^{\chi_{2B}} & \text{if} \quad P < P_{eq2}(T) \text{ and } C_2(t) \geq 0 \end{cases} \qquad 3.1\text{-}4b$$

By Eq. 3.1-1

$$\frac{dC_2}{dt} = -\frac{1}{3}\left(\frac{dC_1}{dt} + \frac{dC_3}{dt}\right) \text{ or } C_2 = C_{2\,0} - \frac{1}{3}\left[\left(C_1 - C_{1\,0}\right) + \left(C_3 - C_{3\,0}\right)\right] \qquad 3.1\text{-}4c$$

where: C_1 = Concentration of $NaAlH_4$ [mole/m^3]
C_2 = Concentration of Na_3AlH_6 [mole/m^3]
C_3 = Concentration of NaH [mole/m^3]

Based on data for the loading of NaH, expressions for $C_{2\,sat}(T)$ and $C_{3\,sat}(T)$, in [mole/m^3], were estimated by UTRC in Attachment 1 as

$C_{2\,sat}(T) = 0$

$$C_{3\,sat}(T) = r_{sat}\left(1 - \frac{wf_{iso}^{sat}(T)}{0.056}\right) \qquad 3.1\text{-}5$$

where: $$r_{sat} = \text{Max}\left[1, \left(1 - \frac{0.0373}{0.056 - wf_{iso}^{sat}(T)}\right)\right] \qquad 3.1\text{-}6$$

The values for $wf_{iso}^{sat}(T)$, the saturation hydrogen weight fraction for loading at a fixed temperature T, are listed in Table 3.1-2. Both the Mathcad® kinetics scoping model, and the COMSOL® two and three-dimensional system models, Hardy [2007], use a spline fit to this data with extrapolated values fixed at the endpoints.

Table 3.1-2
Values for $wf_{iso}^{sat}(T)$

T (K)	$wf_{iso}^{sat}(T)$
353.15	0.021
363.15	0.023
373.15	0.029
393.15	0.022
413.15	0.018

The weight fraction of H_2 contained in the sodium alanate metal, based on Eq. 3.1-1, is defined as

$$wf = \frac{\text{Mass of } H_2 \text{ in Metal}}{\text{Equivalent Mass of } NaAlH_4} = \frac{\left(1.5n_{NaAlH_4} + 0.5n_{Na_3AlH_6}\right)M_{H_2}}{n_{NaAlH_4}M_{NaALH_4} + 3n_{Na_3AlH_6}M_{Na_3AlH_6} + n_{NaH}M_{NaH}} = \frac{1.5C_1 + 0.5C_2}{C_{eqv}}\frac{M_{H_2}}{M_{NaAlH_4}} \quad 3.1\text{-}7$$

where:
n_{NaAlH_4} = Number of moles of $NaAlH_4$
$n_{Na_3AlH_6}$ = Number of moles of Na_3AlH_6
n_{NaH} = Number of moles of NaH
M_{NaAlH_4} = Gram molecular weight of $NaAlH_4$ [kg/g-mole]
$M_{Na_3AlH_6}$ = Gram molecular weight of Na_3AlH_6 [kg/g-mole]
M_{NaH} = Gram molecular weight of NaH [kg/g-mole]
M_{H_2} = Gram molecular weight of H_2 [kg/g-mole].

3.2 Alpha Aluminum Hydride Reaction

The reaction kinetics model for discharge of hydrogen from α-AlH_3 is based on Graetz and Reilly [2005]. Data was used to fit the constants E_a and A in the reaction rate k(T), which is given by

$$k(T) = A\exp\left(-\frac{E_a}{RT}\right) \quad 3.2\text{-}1$$

where:
A = Constant [1/s]
R = Gas constant = 8.314 $\frac{J}{mol\ K}$
E_a = Activation energy [J/mol]
T = Temperature [K].

The rate of decomposition of α-AlH_3 is obtained in terms of the fractional decomposition, α, where

$$\alpha \equiv \frac{n_{AlH_3\,0} - n_{AlH_3}(t)}{n_{AlH_3\,0}} \qquad 3.2\text{-}2$$

So that,

$$\frac{d\alpha}{dt} \equiv \frac{d}{dt}\left[\frac{n_{AlH_3\,0} - n_{AlH_3}(t)}{n_{AlH_3\,0}}\right] = -\frac{d}{dt}\left[\frac{n_{AlH_3}(t)}{n_{AlH_3\,0}}\right] \qquad 3.2\text{-}3$$

where: $n_{AlH_3\,0}$ = Initial number of moles of AlH_3

$n_{AlH_3}(t)$ = Number of moles of AlH_3 at time t.

α is expressed as

$$\alpha = 1 - \exp\left(-Bt^n\right) \qquad 3.2\text{-}4$$

where: $k(T) \equiv B^{1/n}$ or $B = k(T)^n$ 3.2-5

Then, from Equations 3.2-4 and 3.2-5

$$\alpha = 1 - \exp\left(-\left[k(T)t\right]^n\right) \qquad 3.2\text{-}6$$

Graetz and Reilly found that $n \approx 2$ and for α-AlH_3, $A = 1.2 \times 10^{10}\ (s^{-1})$ and $E_a = 102.2 \times 10^3\ J/mol$.

Hence, from Equations 3.2-3 and 3.2-6

$$\frac{d}{dt} n_{AlH_3}(t) = 2n_{AlH_3\,0}\left(k(T)^2 t\right)\exp\left[-\left(k(T)t\right)^2\right] \qquad 3.2\text{-}7$$

Equation 3.2-1, along with the values for A and E_a, is used to provide an explicit expression for k(T).

4.0 DESCRIPTION OF GEOMETRY AND HEAT REMOVAL SCOPING MODEL

The size of a hydrogen storage system, the location of particular components and it gravimetric and volumetric capacities are calculated with the geometry scoping model. Operating parameters for the heat removal system are calculated with the heat removal parameter scoping model. The heat transfer scoping model inputs data from the geometry scoping model and is therefore run afterwards. Although the two scoping models are distinct, they are both incorporated in to the same Microsoft Excel®

workbook, using the workbook format to transfer necessary data from the geometry scoping model to the heat transfer scoping model.

4.1 Geometry Scoping Model

The storage system modeled in this report consists of a cylindrical bed with a circular array of axial coolant tubes and a central axial coolant tube, see Figure 4.1.1-1. Fins used to enhance heat transfer, are positioned normal to the vessel axis. The arrangement of fins is similar to that of the UTRC™ storage vessel shown in Figure 2.0-1. The storage media ($TiCl_3$ catalyzed $NaAlH_4$) is layered between the fins. Hydrogen is assumed to be introduced to the bed by a circular array of axial tubes that could be filled with an inert porous metal. The pressure vessel wall is assumed to have a cylindrical midsection with hemispherical end caps.

4.1.1 Radius of Outer Coolant Tube Ring

Consider a cylindrical bed having a cross-sectional geometry similar to that in Figure 4.1.1-1, but with a variable number of coolant and hydrogen feed tubes. Figure 4.1.1-1 represents a cross-section of the hydride bed only; the pressure vessel, liner and gaps are not included in the drawing. Area A_1 [m^2] in the figure represents the cross-sectional surface area extending from the center of the bed to the circle passing through the centers of the coolant tubes. Area A_2 [m^2] represents the area of the bed extending from the circle passing through the centers of the coolant tubes to the outer edge of the bed.

Let
S_1 = The arc length of tubes in contact with coolant, lying within area A_1.
S_2 = The arc length of tubes in contact with coolant, lying within area A_2.

To obtain similar rates of heat removal for the inner and outer volumes of the bed (which are the volumes formed by projecting areas A_1 and A_2 along the axis of the bed) it is desirable to have

$$\frac{A_1}{S_1} = \frac{A_2}{S_2} \qquad 4.1.1\text{-}1$$

Equation 4.1.1-1, which gives the radius, r of the ring of outer coolant tubes is equivalent to requiring the ratio of volume to cooled surface area to be the same for both regions. This can easily be seen by multiplying the numerator and denominator of both sides of the equation by the bed length, L_{bed}.

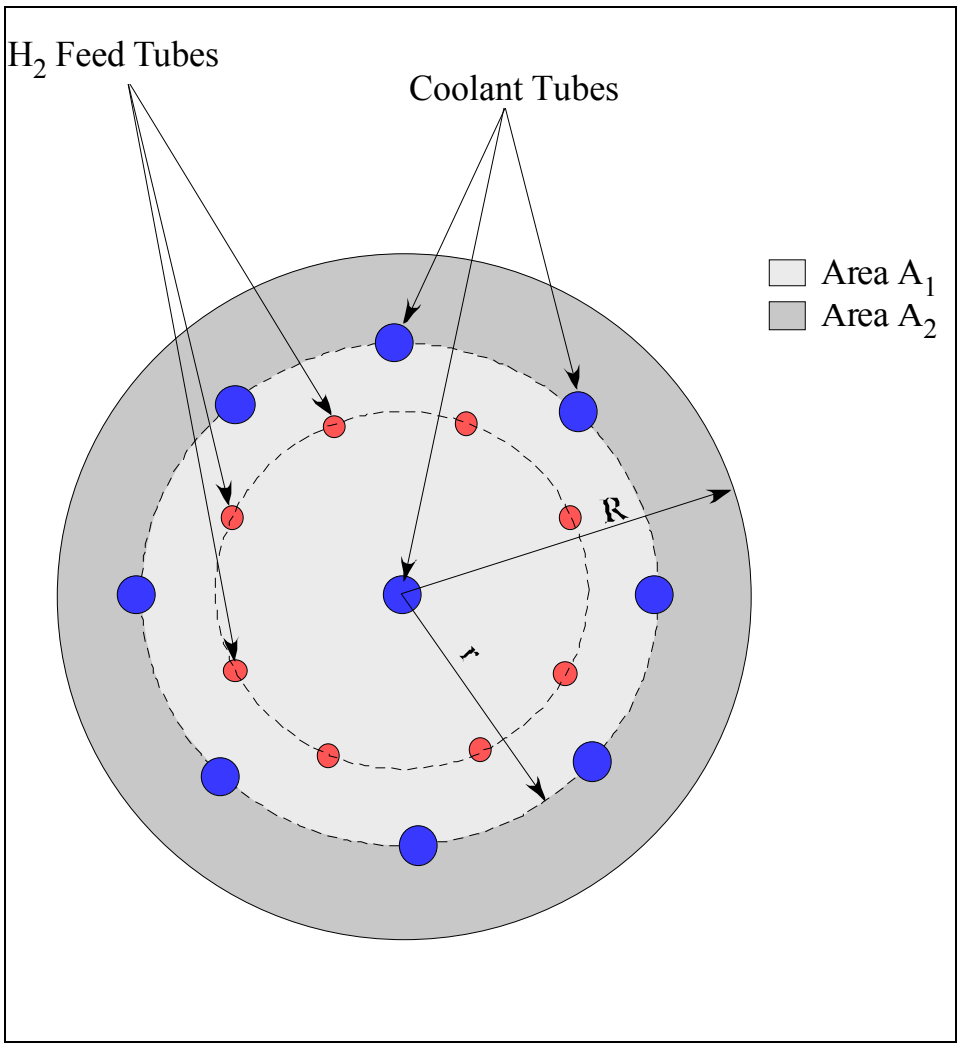

Figure 4.1.1-1 Schematic of bed cross-section. The pressure vessel, liner and any gaps are not included. The number of coolant tubes and hydrogen feed tubes may vary.

The arc lengths of the surfaces in contact with the coolant, S_1 and S_2, in [m],are calculated by considering the geometries shown in Figure 4.1.1-2 and Figure 4.1.1-3.

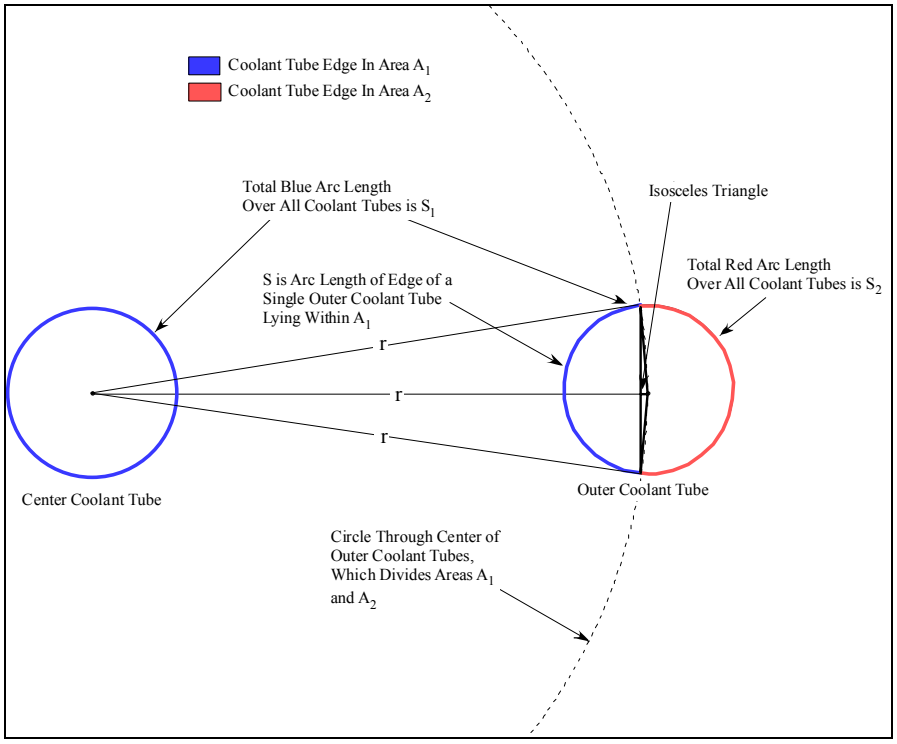

Figure 4.1.1-2 Geometry for the partition of the cooled tube surface with respect to the inner and outer areas of the bed. Figure is not to scale.

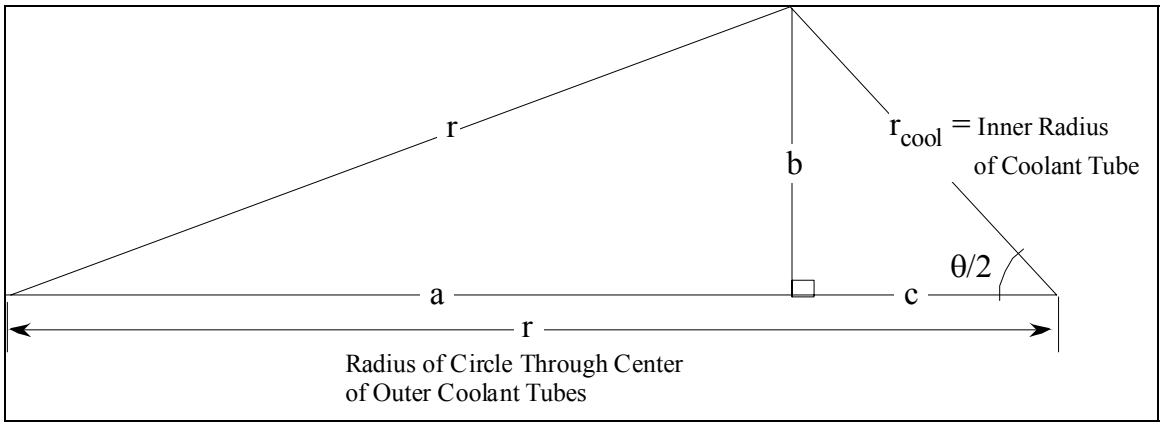

Figure 4.1.1-3 Schematic expansion of upper half of isosceles triangles formed by the center coolant tube and outer coolant tube, and within the outer coolant tube, see Figure 4.1.1-2.

From Figures 4.1.1-2 and 4.1.1-3

$$r^2 = a^2 + b^2 \qquad 4.1.1\text{-}2$$

$$r_{cool}^2 = c^2 + b^2 \qquad 4.1.1\text{-}3$$

$$r = a + c \qquad 4.1.1\text{-}4$$

Solve for a from Equations 4.1.1-2 through 4.1.1-4

$$a = \frac{2r^2 - r_{cool}^2}{2r} \qquad 4.1.1\text{-}5$$

So, from Equation 4.1.1-2

$$b = \frac{r_{cool}}{2}\sqrt{\left(4r^2 - r_{cool}^2\right)} \qquad 4.1.1\text{-}6$$

Now, θ (in radians), shown in Figure 4.1.1-3, is

$$\theta = 2\arcsin\left(\frac{b}{r_{cool}}\right) = 2\arcsin\left(\frac{1}{2r}\sqrt{\left(4r^2 - r_{cool}^2\right)}\right) \qquad 4.1.1\text{-}6$$

The arc length, S [m], of the edge of a single outer coolant tube lying within area A_1, see Figure 4.1.1-2, is

$$S = r_{cool}\theta = 2r_{cool}\arcsin\left(\frac{1}{2r}\sqrt{\left(4r^2 - r_{cool}^2\right)}\right) \qquad 4.1.1\text{-}8$$

The total arc length, S_1 [m], of the edges of all coolant tubes lying within area A_1 is

$$S_1 = \left(n_{cool} - 1\right)S + \pi D_{cool} \qquad 4.1.1\text{-}9$$

The total arc length, S_2 [m], of the edges of all coolant tubes lying within area A_2 is

$$S_2 = \left(n_{cool} - 1\right)\left(\pi D_{cool} - S\right) \qquad 4.1.1\text{-}10$$

where: n_{cool} = Total number coolant tubes
D_{cool} = Inner diameter of coolant tube [m].

The areas A_1 and A_2 are given by

$$A_1 = \pi r^2 - \pi\left(\frac{D_{cool\_outer}}{2}\right)^2 - n_{H_2}\pi\left(\frac{D_{H_2}}{2}\right)^2 - \left(n_{cool} - 1\right)\frac{\theta}{2}\left(\frac{D_{cool\_outer}}{2}\right)^2 \qquad 4.1.1\text{-}11$$

$$A_2 = \pi\left(R^2 - r^2\right) - \left(n_{cool} - 1\right)\left(\frac{D_{cool\_outer}}{2}\right)^2\left(\pi - \frac{\theta}{2}\right) \qquad 4.1.1\text{-}12$$

where: n_{H_2} = Total number hydrogen feed tubes
D_{H_2} = Inner diameter hydrogen feed tube [m]

D_{cool_outer} = Outer diameter of coolant tube, including sleeve formed by extrusion of fin [m].

To satisfy Equation 4.1.1-1 the following must be valid, with substitutions from Equations 4.1.1-9 through 4.1.1-12

$$\frac{A_1}{S_1} - \frac{A_2}{S_2} = 0 \qquad 4.1.1\text{-}13$$

Given the total number of coolant and hydrogen feed tubes, along with their associated dimensions, Equation 4.1.1-13 is used as an objective function in the Excel® spreadsheet to obtain a value for r.

4.1.2 Length of Bed

The required length, L_{hyd}, of the hydride alone, without vessel walls, liners or fins, is

$$L_{hyd} = \frac{V_{hyd}}{\pi\left[R^2 - n_{cool}\left(\frac{D_{cool\_outer}}{2}\right)^2 - n_{H_2}\left(\frac{D_{H_2}}{2}\right)^2\right]} \qquad 4.1.2\text{-}1$$

where: V_{hyd} = Total volume of hydride (in a reference chemical form) [m^3]. Depends on hydride density, mass of hydrogen to be stored and moles of recoverable hydrogen to the moles of $NaAlH_4$.

For a bed with fins bounding the end surfaces, having a thickness t [m], and approximate spacing δ_{approx} [m], the number of plate fins, n_{plate}, is given by

$$n_{plate} = \text{Roundup}\left(\frac{L_{hyd}}{\delta_{approx}}, 0\right) + 1 \qquad 4.1.2\text{-}2$$

Here, the operator *Roundup(x,0)* in Excel® rounds x up to the next highest integer.

Given this number of fins, the total length of the bed, including hydride and fins, is

$$L_{hyd\&fins} = L_{hyd} + tn_{plate} \qquad 4.1.2\text{-}3$$

The actual spacing between the fins, δ [m], (which is the axial distance between the surfaces of the fins bounding the metal hydride layer) is

$$\delta = \frac{L_{hyd\&fins} - tn_{plate}}{n_{plate} - 1} \qquad 4.1.2\text{-}4$$

4.1.3 Input Parameters for System Dimensions

The input parameters required to calculate the dimensions of the storage vessel are list in Table 4.1.3-1.

Table 4.1.3-1 Input for Calculation of System Dimensions

Parameter	Value
Mass of recoverable H_2 to be stored in vessel	1000.00 g
Practical ratio of moles H_2 to moles $NaAlH_4$ that can be stored	1.500
Bulk density of $NaAlH_4$ powder	0.72 g/ cm^3
Hydride bed diameter, no walls	23.00 cm
Diameter of coolant tubes	1.91 cm
Diameter of H_2 injection tubes	1.27 cm
Number of coolant tubes	9
Number of H_2 injection tubes	8
Thickness of fin plates	0.0313 cm
Approximate spacing between fin plates	0.64 cm
Tube wall thickness	0.12 cm
Density of tube material (6061-T6 Al from table on pg 6-11 of Avallone and Baumeister [1987])	2.70 g/ cm^3
Density of fin material (6061-T6 Al from table on pg 6-11 of Avallone and Baumeister [1987])	2.70 g/ cm^3
Material density of porous insert for H_2 delivery (6061-T6 Al from table on pg 6-11 of Avallone and Baumeister [1987])	2.70 g/ cm^3
Void fraction of porous insert for H_2 delivery	0.70
Density of tank material (Composite @ 0.05419lbm/in^3)	1.50 g/ cm^3
Density of liner material (6061-T6 Al from table on pg 6-11 of Avallone and Baumeister [1987])	2.70 g/cm^3
Assume 1/16 in gap between bed & liner	0.159 cm
Assume 1/32 in thick liner	0.079 cm
Tank wall thickness at 50 bar w/ safety factor	0.132 cm

4.1.4 Bed Characteristics

The Department of Energy has set goals for the system volumetric capacity, V_{cap}, and the system gravimetric capacity, G_{cap}, which are respectively defined as

$$V_{cap} \equiv \frac{m_{H_2}}{V_{system}} \qquad 4.1.4\text{-}1$$

and

$$G_{cap} \equiv \frac{m_{H_2}}{m_{system}} \qquad 4.1.4\text{-}2$$

where: m_{H_2} = Mass of recoverable hydrogen reacted in the bed [kg].

V_{system} = Total volume of storage tank, including the bed, fins, liner gaps and pressure vessel [m^3].

m_{system} = Total mass of loaded storage tank, including the bed loaded with H_2, fins, liner gaps and pressure vessel. The mass of the heat transfer fluid is not included [kg].

V_{cap} and G_{cap} are calculated in the scoping spreadsheet.

4.2 Heat Transfer Parameters

The exothermic chemical reactions occurring during the loading of the bed and the requirement that the bed be heated to release hydrogen necessitate the use of a heat management system. Since a shell and tube heat transfer system is assumed for the storage system, the principal heat transfer parameters are those related to convective exchange within the coolant tubes.

In the spreadsheet model, the required rate of heat removal is determined by dividing the total heat generated during the charging of the bed by amount of time required for charging to occur. In this calculation, it is tacitly assumed that heat transfer to the coolant tubes is instantaneous and that the bed uptakes the full charge of hydrogen over the time allotted for charging. The system modeled in this report was evaluated for Dowtherm T® heat transfer fluid for single phase cooling and DuPont Vertrel-XF® heat transfer fluid for two phase cooling. Data sheets, from the respective vendors are listed in Attachments 1 and 2.

4.2.1 Single Phase Flow

For coolant in single phase flow the Dittus-Boelter correlation was used to predict the mass flowrate required to remove the heat of reaction. From Holman [1976] the Dittus-Boelter correlation is

$$Nu_D = 0.023\,Re^{0.8}\,Pr^{0.4} \qquad 4.2.1\text{-}1$$

where: $Nu_D = \frac{h_{DB}D}{k_f}$ = Nusselt number based on diameter, D

D = Inner diameter of coolant tube [m]

h_{DB} = Dittus-Boelter convection heat transfer coefficient for the heat transfer fluid [W/(m^2- K)]

k_f = Thermal conductivity of the heat transfer fluid [W/(m- K)]

$Re_D = \frac{GD}{\mu}$ = Reynolds number based on diameter, D

G = Coolant mass flux [kg/(m^2-s)]

μ = Viscosity [Pa-s]

$Pr = \frac{\nu}{\alpha}$ = Prandtl number

ν = Kinematic viscosity of coolant [m^2/s]

α = Thermal diffusivity of coolant [m^2/s].

Therefore, the single phase convection heat transfer coefficient, h_f, is that obtained from the Dittus-Boelter correlation, h_{DB}, which is

$$h_{DB} = 0.023\left(\frac{GD}{\mu}\right)^{0.8} Pr^{0.4}\,\frac{k}{D} \qquad 4.2.1\text{-}2$$

The average heat flux, q", from the wall of the coolant tube is then

$$q" = h_{DB}\left(T_{wall} - T_{bulk}\right) = \left(0.023\left(\frac{GD}{\mu}\right)^{0.8} Pr^{0.4}\,\frac{k}{D}\right)\left(T_{wall} - T_{bulk}\right) \qquad 4.2.1\text{-}3$$

where: T_{wall} = Tube wall temperature (K).
T_{bulk} = Bulk coolant temperature (K).

Based on the stored mass of hydrogen, m_{H_2}, and the time, τ, for the loading process, the average heat flux is

$$q" = \frac{\left(m_{H_2} / M_{H_2}\right)\Delta H_{rx}}{\tau} \qquad 4.2.1\text{-}4$$

where: m_{H_2} = Mass of hydrogen stored in the bed (kg).
M_{H_2} = Molecular weight of H_2 [kg/g-mol].
ΔH_{rx} = Overall heat of reaction for uptake of H_2 by the hydride [J/g-mol].
τ = Time required for H_2 loading [s].

Use Equations 4.2.1-3 and 4.2.1-4 to obtain the mass flux, G, required to remove the heat generated during loading.

$$G = \frac{(q")^{1/0.8}}{\left[0.023\,\frac{k}{D}\,Pr^{0.4}\left(\frac{D}{\mu}\right)^{0.8}\left(T_{wall} - T_{bulk}\right)\right]^{1/0.8}} \qquad 4.2.1\text{-}5$$

The pressure drop over the length of a coolant tube (length of the bed), required to drive coolant through the tube at a mass flux G, is

$$\Delta P = f\,\frac{L_{hyd\&fins}}{D}\,\frac{G^2}{2\rho} \qquad 4.2.1\text{-}6$$

where: f = Friction factor for the tube
ΔP = Pressure drop across the length of the tube [Pa]
$L_{hyd\&fins}$ = Length of the bed, including hydride and fins [m].

The rise in the bulk coolant temperature over the length of a coolant tube (length of the bed) is approximated as

$$\Delta T \approx 4\frac{q''L_{hyd\&fins}}{DGC_p} \qquad 4.2.1\text{-}7$$

where: C_p = Specific heat of coolant [J/(kg-K)], assumed approximately constant
ΔT = Change in bulk temperature of coolant over the length of the bed [K].

4.2.2 Two Phase Flow

If the coolant is allowed to boil at the inner wall of the coolant tube, and the critical heat flux is not exceeded, the rate of wall heat transfer will be greater than if the coolant remained in the liquid state. However, the chemical kinetics of the bed are dependent on temperature. Thus, the coolant must be selected to have a saturation temperature that is consistent with optimal reaction rates in the bed.

Gungor and Winterton [1986] adapted their correlation for the convection heat transfer coefficient in vertical two-phase flow to horizontal flows by identifying a liquid Froude number dependent threshold between stratified and non-stratified flows. The liquid Froude number, Fr_L, is defined as

$$Fr_L = \frac{G^2}{\rho_L^2 gD}(1-x)^2 \qquad 4.2.2\text{-}1$$

where: G = Mass flux of liquid and gas phases of coolant, [kg/m^2-s]
g = Gravitational acceleration [m/s^2]
D = Inner diameter of coolant tube [m]
ρ_L = Density of saturated liquid coolant [kg/m^3]
x = Quality of coolant $\left[\frac{\text{Mass of Gas Phase of Coolant}}{\text{Mass of Coolant}}\right]$

When $Fr_L > 0.05$, the 1986 Gungor and Winterton vertical flow correlation is used directly, otherwise multipliers were used to modify terms in the correlation.

The Gungor and Winterton [1986] correlation for the convection heat transfer coefficient depends on the coolant gas phase viscosity through the Martinelli parameter. Unfortunately, data for the gas phase viscosity of the selected coolant, DuPont Vertrel-XF®, was unavailable. Therefore, in place of the Gungor and Winterton [1986] correlation, the Gungor and Winterton [1987] correlation was used because it was not dependent on the gas phase viscosity. The Gungor and Winterton [1987] correlation

$$\text{was } h_{2\phi} = \left[1 + 3000B^{0.86} + 1.12\left(\frac{x}{1-x}\right)^{0.75}\left(\frac{\rho_L}{\rho_V}\right)^{0.41}\right]h_{DBL} \qquad 4.2.1\text{-}2$$

where: $h_{2\phi}$ = Two phase convection heat transfer coefficient [W/m^2 K]
ρ_V = Density of saturated vapor [kg/m^3]

h_{DBL} = Dittus-Boelter convection heat transfer coefficient based on the local properties of the liquid coolant [W/m^2 K]

$$= 0.023\,Re_L^{0.8}\,Pr_L^{0.4}\left(\frac{k_L}{D}\right) \qquad 4.2.1\text{-}2$$

k_L = Thermal conductivity for the saturated liquid coolant [W/m-K]

Re_L = Reynolds number for the liquid coolant = $\dfrac{G(1-x)D}{\mu_L}$ 4.2.1-3

Pr_L = Prandtl number for the liquid coolant = $\dfrac{Cp_L\mu_L}{k_L}$ 4.2.1-4

μ_L = Viscosity of the saturated liquid coolant [Pa-s]

Cp_L = Specific heat of the saturated liquid coolant [J/kg K]

$$B = \frac{q''}{Gh_{lg}} \qquad 4.2.2\text{-}5$$

q" = Heat flux at tube wall [W/m^2]

h_{lg} = Enthalpy of phase change for the coolant [J/kg].

The heat flux at the inner wall of the coolant tube is given by

$$q'' = h_{2\phi}(T_w - T_{sat}) \qquad 4.2.2\text{-}6$$

where: q" = Heat flux at inner wall of coolant tube [W/m^2]

T_w = Temperature of the inner wall of the coolant tube [K]

T_{sat} = Saturation temperature of the coolant [K]

For fixed values of q" and $(T_w - T_{sat})$, Equations 4.2.2-2 through 4.2.2-6 can be used to obtain the coolant mass flux, G via the iterative solver in Microsoft Excel®.

4.2.3 Input for Heat Transfer

The input required to calculate heat transfer requirements for the system are listed in Table 4.2.3-1

Table 4.2.3-1 Input for Calculation of Heat Transfer Parameters

Parameter	Value	Reference
ΔH_{Rxn1}	37.00 kJ/mol H2	Heat of reaction from species 2 to species 1, see Eq. 3.1-1, Gross [2003]
ΔH_{Rxn2}	47.00 kJ/mol H2	Heat of reaction from species 3 to species 2 , see Eq.3.1-1, Gross [2003]
Charging Time	180.00 sec	
Wall Temp	90.00 °C	
2ϕ Coolant Liquid Density	1580 kg/m^3	DuPont Vertrel-XF®, see Attachment 2
2ϕ Coolant Vapor Density	1.01 kg/m^3	DuPont Vertrel-XF®, see Attachment 2
2ϕ Coolant Liquid Themal Cond	10.4 W/(m K)	DuPont Vertrel-XF®, see Attachment 2
2ϕ Coolant Liquid Viscosity	0.001 kg/(m s)	DuPont Vertrel-XF®, see Attachment 2
2ϕ Coolant Liquid Specific Heat	1130 J/(kg K)	DuPont Vertrel-XF®, see Attachment 2
2ϕ Coolant Phase Change Enthalpy	129800 J/kg	DuPont Vertrel-XF®, see Attachment 2
2ϕ Coolant Liquid Prandtl No.	7.29	DuPont Vertrel-XF®, see Attachment 2
Void Fraction (ε)		
Quality (x)		
1ϕ Coolant Liquid Density	820 kg/m^3	Dowtherm T®, see Attachment 1
1ϕ Coolant Liquid Themal Cond	0.104 W/(m K)	Dowtherm T®, see Attachment 1
1ϕ Coolant Viscosity	0.003 kg/(m s)	Dowtherm T®, see Attachment 1
1ϕ Coolant Specific Heat	2300 J/(kg K)	Dowtherm T®, see Attachment 1
1ϕ Coolant Prandtl No.	66.52	Dowtherm T®, see Attachment 1

5.0 RESULTS

Results from the kinetics, geometry and heat transfer scoping models are discussed in the following sections. A full scoping analysis of the sodium alanate bed was performed, while only the kinetics of the alpha-aluminum hydride bed were evaluated.

5.1 Kinetics Model

In this report, the Mathcad® based kinetics model was applied to $TiCl_3$ catalyzed $NaAlH_4$ and to α-AlH_3. Charging and discharging rates calculated by the kinetics model were idealized because the temperature and pressure remained fixed throughout the process; quite different from what would occur in an actual storage bed. In an actual storage bed, there will be a transient change in the pressure when the bed is charged or discharged. Further, thermal inertia coupled with heat generated by chemical reactions will result in spatial variation in the temperature of the bed. The pressure and temperature variations from fixed values will result in variations from the reaction rates predicted by the Mathcad® model. These effects are the primary reason that a 3-dimensional model that

couples thermal, mass and momentum transport is required to provide a more accurate assessment of bed peformance. However, because the temperature and pressure are fixed in the Mathcad® kinetics model, it can be used to predict the upper limit for loading and discharge for a particular storage media. In addition to reaction rates, the kinetics model can be used to predict both the long-time capacity of a storage media, as well as the best case loading for the allotted refueling time period.

5.1.1 $TiCl_3$ Catalyzed $NaAlH_4$

At 68 bar, the UTRC™ kinetics model for $TiCl_3$ catalyzed $NaAlH_4$ from Attachments 3 and 4, gave the hydrogen uptake rates shown in Figure 5.1.1-1. Loading rates in this figure are expressed in terms of the weight fraction of hydrogen stored in the hydride, see Equation 3.1-7. This result identical to the rates obtained from UTRC™, see the reports in Attachments 3 and 4 and Figure 5.1.1-2.

Loading a bed initially composed of pure NaH, with an excess of Al, at 50 bar and 100°C. gives the loading curve shown in Figure 5.3.1-3. The bed gravimetric capacity, which is the maximum weight fraction, approaches 0.029 at the long time limit, rather than 0.056, which is the theoretical limit based on the chemical balance in Equation 3.1-1.

Cycling a bed having an initial concentration of 13,333.33 mole/m^3 of NaH, and 0 mole/m^3 of the other hydrides, with a stoichiometric quantity of Al, between loading and discharging conditions, of 100°C at 50 bar and 120°C at 1 bar, respectively, gives the concentration curves shown in Figure 5.1.1-4.

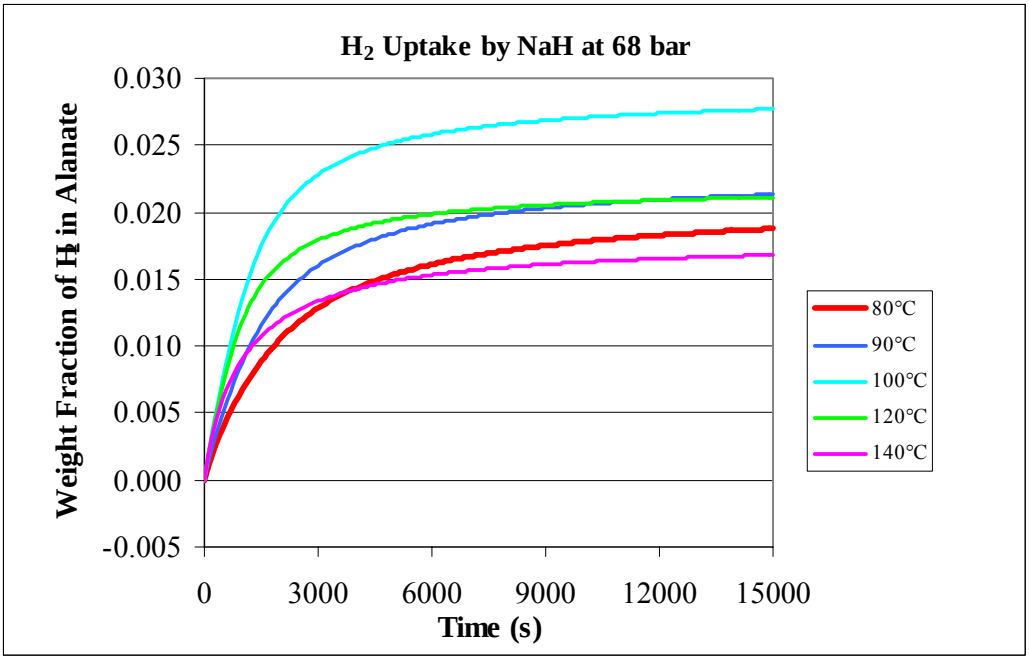

Figure 5.1.1-1 Hydrogen loading rates at 68 bar from the Mathcad® reaction kinetics model.

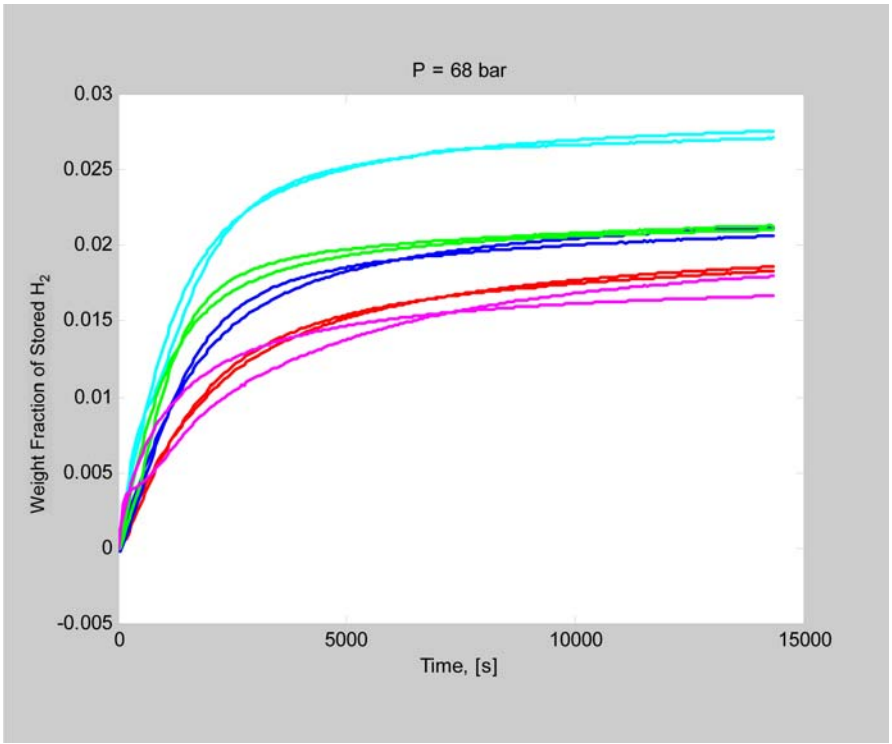

Figure 5.1.1-2 Hydrogen loading rates at 68 bar from the UTRC™ reaction kinetics model in Attachments 3 and 4. Solid lines represent data and dashed lines

represent the model. The legend of Figure 5.3.1-1 gives the loading temperatures

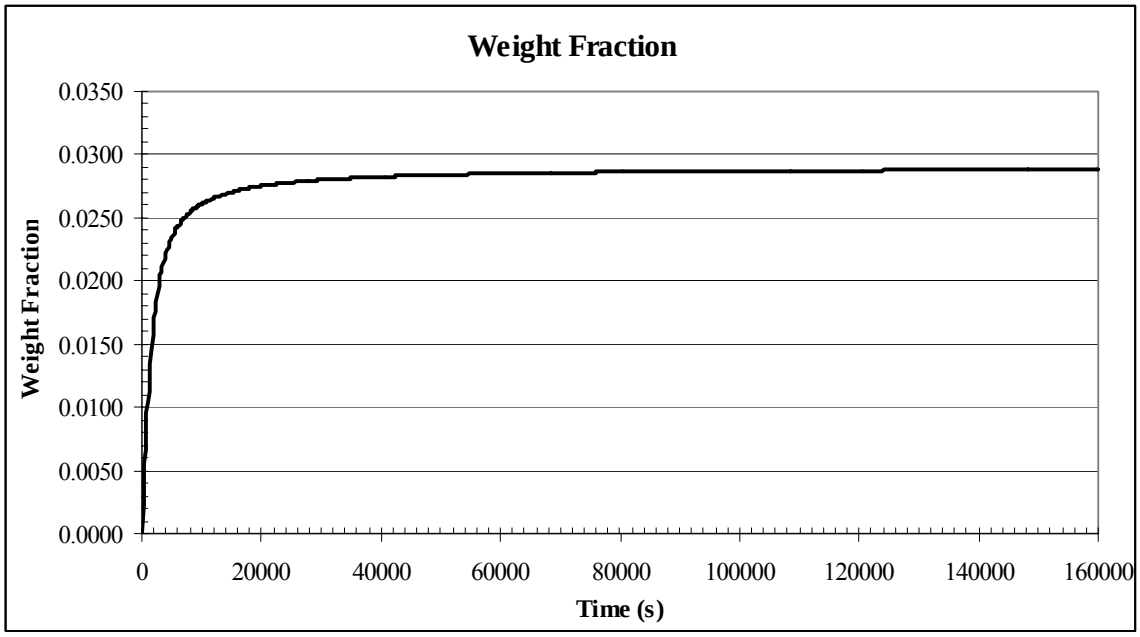

Figure 5.1.1-3 Loading of hydrogen in the hydride at 50 bar and 100°C. Storage in both $NaAlH_4$ and Na_3AlH_6 are included.

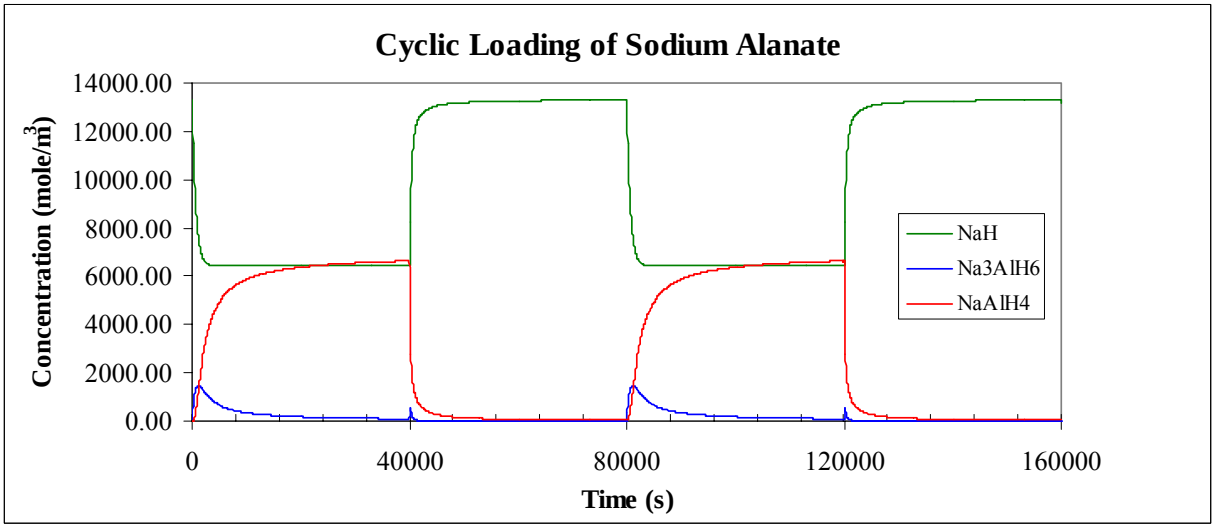

Figure 5.1.1-4 Concentration of all species in the sodium alanate reaction. The initial concentration of NaH was 13,333.33mole/m^3 and 0 mole/m^3 for the other hydrides.

5.1.2 α-AlH_3 Discharge Kinetics

Due to the unavailability of loading kinetics for α-AlH_3, only the discharge rates were modeled, using the kinetics proposed by Graetz and Reilly [2005]. The kinetics for this process were independent of pressure, hence, only the effect of temperature was considered.

The rate of decomposition of α-AlH_3, relative to the initial concentration, at constant temperature is given by the family of curves in Figure 5.3.2-1. The corresponding rate of H_2 release, in units of $\frac{\text{mole } H_2}{(\text{mole } \alpha - AlH_{3\,0})*\text{second}}$, is shown in Figure 5.1.2-2.

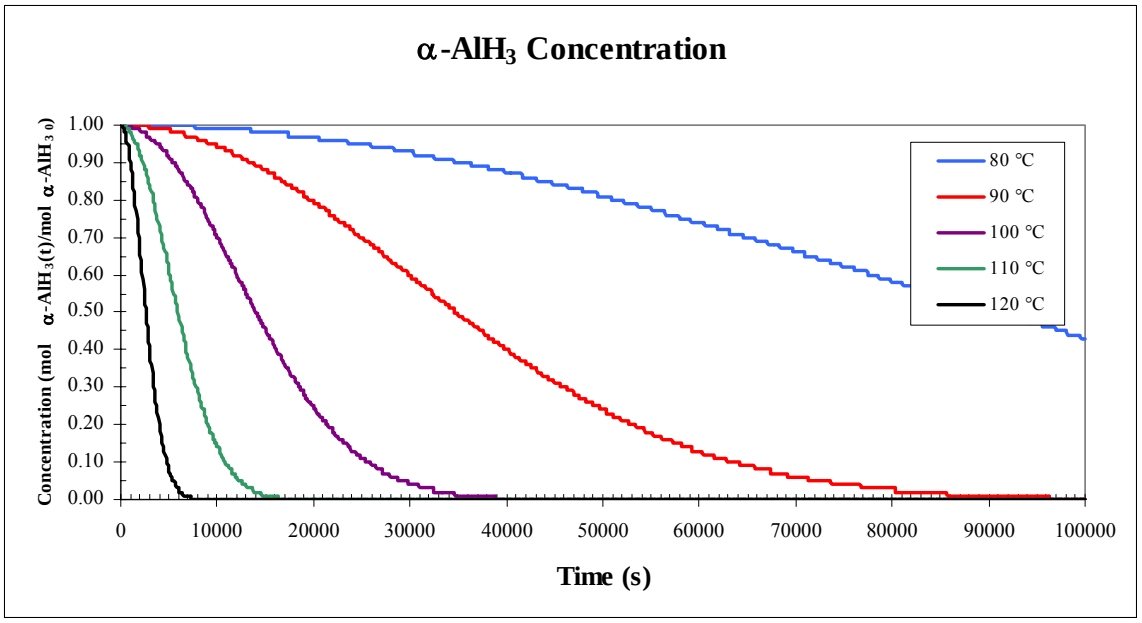

Figure 5.1.2-1 Decomposition of α-AlH_3 in terms of relative concentration, with respect to the initial concentration of α-AlH_3.

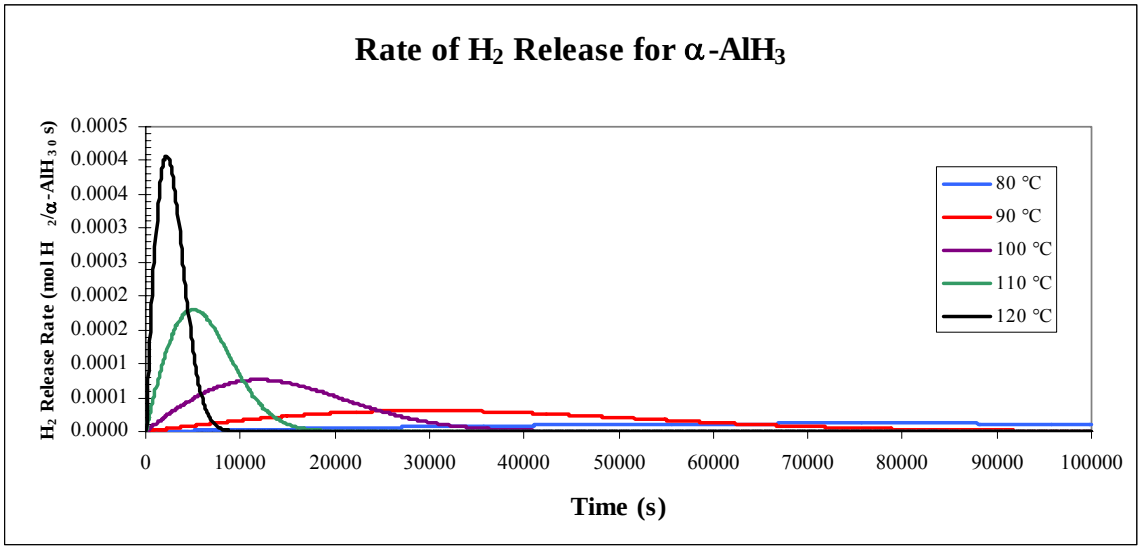

Figure 5.1.2-2 Rate of H_2 generation due to decomposition of α-AlH_3. The rate is expressed in terms of the rate of H_2 produced relative to the initial concentration of α-AlH_3.

5.2 Bed Geometry

Appendix A.1 contains a copy of the input and output used in the Microsoft Excel® spreadsheet used for scoping calculations related to the sodium alanate bed geometry. Due to the low loading rate predicted by the kinetics model, the time allowed for charging the bed was 12 minutes, rather than the DOE 2007 technical target of 10 minutes. In this sample calculation, however, the ratio of moles of recoverable H_2 to moles of $NaAlH_4$ in the fully converted bed was input as 1.5 rather than 0.213, which is the value calculated by the kinetics scoping model for a 12 minute charging time, see Table 4.1.3-1. Based on the model input, the parameters in Table 5.2-1 were obtained.

Table 5.2-1 Calculated Bed and Vessel Parameters

Required length of hydride alone (no structural members, fins or vessel)	0.6562 m
Total number of fin plates, including ends	105
Total length of bed (with fins but no vessel)	0.6890 m
Actual spacing of plates	0.0063 m
Mass of bed; including fins, tubes & $NaAlH_4$	24.643 kg
Volume of bed with vessel & liner	0.0362 m^3
Overall length of vessel (assumed semi-spherical ends)	0.9264 m
Radial distance from axis of storage vessel to center of cooling tube circle. The distance r in Figure 4.1.1-1	0.0855 m
Gravimetric capacity of storage system	0.041 (kg H_2)/(kg Total)
Volumetric capacity of storage system	0.028 (kg H_2)/(L Total)

5.3 Bed Heat Transfer

The spreadsheet used to compute input and output for the loading phase bed heat transfer requirements is listed in Appendix A.2. For sodium alanate, loading heat transfer requirements were chosen because they present the greatest challenge to the heat removal system. The spreadsheet contains the input required for the sodium alanate system evaluated in this report and references the bed geometry model listed in Appendix A.1. Predicted system heat transfer parameters are also contained in the spreadsheet listed in Appendix A.2.

Based on the chemical reaction equation and heats of reaction for $NaAlH_4$, the time required for loading (12 minutes) and the surface area of the coolant tubes, the surface heat flux at the interior wall of a coolant tube was calculated to be 3.45×10^5 W/m^2.

5.3.1 Single Phase Flow

For single phase flow the heat transfer fluid considered was Dowtherm T®, having properties listed in Table 4.2.3-1. For this heat transfer fluid, the operating parameters required to remove the heat of reaction during loading are listed in Table 5.3.1-1. The required mass flux of coolant was computed using the Dittus-Boelter correlation, see Holman [1976].

Table 5.3.1-1 Bed Heat Removal Parameters for a Single Coolant Tube

Parameter	Value
Mass Flux	10,300.4 kg/(m^2 s)
Mean Flow Velocity	12.61 m/s
Tube Reynolds Number	58,861.02
Pressure Drop Over Length of Tube	8.134×10^4 Pa
Increase in Temperature Over Length of Tube	2.42 °C

5.3.2 Two-Phase Flow

In an attempt to enhance heat transfer from the bed during loading, cooling by two phase flow was investigated. The heat transfer fluid considered in the model was DuPont Vertrel-XF® and the required two phase mass flux was calculated from the Gungor-Winterton correlation [1986], assuming a low inlet quality for the coolant (on the order of 10^{-5}). The required mass flux for two phase flows was calculated to be 16703.9 kg/(m^2 s).

Enhanced heat removal by the coolant is only effective if it is consistent with the rate of heat transfer from the hydride bed. The ratio of the rate of heat removal by convection in the coolant to heat transfer by conduction by the bed is given by the Biot modulus, Bi. The Biot modulus is defined as

$$\mathrm{Bi} = \frac{h_{conv} L}{k_{bed}}, \qquad 5.2.2\text{-}1$$

where: h_{conv} = Convection heat transfer coefficient for the coolant [W/(m^2-K)]
k_{bed} = Thermal conductivity of the metal hydride bed [W/(m-K)].
L = Characteristic length [m].

For the two-phase cooled system analyzed in this report, see Appendix A.2
$h_{2\phi} = h_{conv\,cool} = 0.9929$ W/(cm^2-°C) = 9929 W/(m^2-K)

and, from Mosher, et. el. [2007]
$k_{bed} = 0.325$ W/m-K

Take L to be the distance from the center coolant tube to a coolant tube in the ring, see Figure 4.1.1-1 and Appendix A.1. Then
$L \approx r - D \approx 0.076$ m

and,
$Bi \approx 2{,}322$.

For a large Biot modulus, the rate of heat removal by convection far exceeds that by conduction. This implies that heat removal from the bed is limited by conduction and that the use of two-phase cooling alone will not improve heat removal for the bed configuration evaluated in this report. For this system geometry and storage material, it is more important to reduce the conduction transport length in the bed, L, or increase the bed thermal conductivity than to enhance convection heat transfer.

6.0 CONCLUSIONS

The kinetics, geometry and heat transfer, scoping models developed in this task can be used to quickly assess whether or not a hydrogen storage system meets operational requirements and should be evaluated with a more detailed model. Further, the scoping models may also be used to identify design modifications that improve performance. While the models do not perform detailed, coupled physics calculations, as would the more complete numerical model discussed in Hardy [2007], they provide sufficient information to estimate the dimensions and heat transfer parameters required for the storage system.

For a particular hydride and bed configuration the kinetics, geometry and heat transfer scoping models are applied in the following sequence. First, the mass of hydride required to store a given amount of hydrogen in the allotted refueling time is calculated with the kinetics model. Optimal temperatures and pressures during the loading and discharge phases are also determined from the model. Next, the required mass of hydride is input to the geometry scoping model via the ratio of moles of stored H_2 to moles of final moles of hydride. The remaining input from Table 4.1.3-1 is then entered. Finally, for a particular heat transfer fluid, the heat transfer requirements for the system are determined from the bed heat transfer scoping model.

When applied to the UTRC™ kinetics correlation for $NaAlH_4$, the kinetics model replicated the UTRC™ predictions, see Figures 5.3.1-1 and 5.3.1-2. Even under the most favorable loading conditions, however, the model showed that the approach to the theoretical weight fraction of stored hydrogen was very slow. Hence, to store sufficient hydrogen in the DOE target refueling time the mass of hydride will need to be increased to the point that the gravimetric capacity of the bed will be far below the DOE 2007 technical target gravimetric capacity of 0.045 for the system. For α-AlH_4, the kinetics model showed that the release rate of hydrogen is very strongly dependent on temperature.

7.0 REFERENCES

COMSOL Multiphysics®, version 3.3.0.405. Copyright 1994-2006, COMSOL AB

Graetz, J. and J. J. Reilly. "Decomposition Kinetics of the AlH_3 Polymorphs." *J. Phys. Chem*., B, **109**, 22181-22185, **2005**.

Gross, K. J. "The Reversible Hydrides Solution for Hydrogen Storage." *Slide Presentation for G-CEP Hydrogen Workshop*, April 14 & 15, **2003**.

Gungor, K. E., and R. H. S. Winterton. "A General Correlation for Flow Boiling in Tubes and Annuli." *Int. J. Heat Mass Transfer*, Vol. 29, 351-358, **1986**.

Gungor, K. E., and R. H. S. Winterton. "Simplified General Correlation for Saturated Flow Boiling and Comparisons of Correlations With Data" *Chem. Eng. Des. Rev.*, Vol. 65, 148-156, **1987**.

Hardy, B. J. "Integrated Hydrogen Storage System Model." *Washington Savannah River Company Document*, WSRC-TR-20007-00440, Rev.1, **2007**.

Holman, J. R. "Heat Transfer." 4th Edition, *McGraw-Hill,* New York **1976**.

Mathcad®, version 14.0.0.163. Copyright © 2007 Parametric Technology Corporation.

Microsoft® Excel **2002** (10.6834.6830) SP3. Microsoft Corporation.

Mosher, D, X. Tang, S. Arsenault, B. Laube, M. Cao, R. Brown and S. Saitta. "High Density Hydrogen Storage System Demonstration Using NaAlH4 Complex Compound Hydrides." *DOE Hydrogen Program Annual Peer Review*, Arlington, VA, **2007**.

APPENDIX

A.1 GEOMETRY AND HEAT REMOVAL SCOPING MODEL REQUIREMENTS

A.1.1 Geometry Scoping Model

The size, number of fins, gravimetric and volumetric capacities of the system evaluated in this report were based on parameters input to the Microsoft Excel® geometry scoping model shown in Figure A.1.1.

Dimensions of Hydride Bed

6/25/2007

Chemical balance equations

$$NaAlH_4 \leftrightarrow \frac{1}{3}Na_3AlH_6 + \frac{2}{3}Al + H_2 \leftrightarrow NaH + Al + \frac{3}{2}H_2$$

(Reaction 1 / Reaction 2 / Species 1 / Species 2 / Species 3)

Input Parameters

M_{H2}	2.016 g/mol	Gram-Molecular Weight of H_2			n_{H2}	496.03 mols	Moles of H_2 to be stored in vessel			
M_{NaAlH4}	54.000 g/mol	Gram-Molecular Weight of $NaAlH_4$			n_{NaAlH4}	330.69 mols	Moles of $NaAlH_4$ required for vessel			
m_{H2}	1000.00 g	Mass of recoverable H_2 to be stored in vessel			m_{NaAlH4}	17857.28 g	Mass of $NaAlH_4$ required for vessel			
n_{H2}/n_{NaAlH4}	1.500	Practical ratio of moles H_2 to moles $NaAlH_4$ that can be stored			V_{NaAlH4}	24801.77 cm^3	Volume of NaAlH4 required to store hydrogen			
ρ_{NaAlH4}	0.72 g/cm^3	Bulk density of NaAlH4 powder								
D	23.00 cm	Hydride bed diameter, no walls		9.06 in						
D_{cool}	1.91 cm	Diameter of coolant tubes								
$D_{H2\ inject}$	1.27 cm	Diameter of H_2 injection tubes								
n_{cool}	9	Number of coolant tubes			A_{cool}	27.36 cm^2	Total area of coolant tube holes			
$n_{H2\ inject}$	8	Number of H_2 injection tubes			A_{H2}	10.13 cm^2	Total area of H_2 injection tube holes			
t	0.0313 cm	Thickness of fin plates	0.0123 in		0.015625					
s	0.64 cm	Approximate spacing between fin plates		0.2500 in	0.333125					
tw	0.12 cm	Tube wall thickness								
ρ_{tube}	2.70 g/cm^3	Density of tube material (6061-T6 Al from table onpg 6-11 of Mark's 9th Ed)								
ρ_{fin}	2.70 g/cm^3	Density of fin material (6061-T6 Al from table onpg 6-11 of Mark's 9th Ed)								
$\rho_{H2\ inject}$	2.70 g/cm^3	Material density of porous insert for H_2 delivery (6061-T6 Al from table onpg 6-11 of Mark's 9th Ed)								
$f_{H2\ inject}$	0.70	Void fraction of porous insert for H_2 delivery								
ρ_{Tank}	1.50 g/cm^3	Density of tank material (Composite @ 0.05419lbm/in^3 from spreadsheet Wu_hydrogen_storage_size_calculation_composite_vessel.xls)								
ρ_{Liner}	2.70 g/cm^3	Density of liner material (6061-T6 Al from table onpg 6-11 of Mark's 9th Ed)								
Gap thickness	0.159 cm	Guess 1/16 in gap								
Liner Thickness	0.079 cm	Guess 1/32 in thick liner								
Tank Wall Thickness	0.132 cm	At 50 bar w/ safety factor-Wu			COMSOL Extrusion					
					1.5625E-04 m					
Calculated Parameters					3.3109E-03 m					
L_{NaAlH4}	65.62 cm	Required length of hydride only								
n_{Plate}	105	Total number of fin plates, including ends								
L_{Total}	68.90 cm	Total length of bed, no vessel	27.13 in	6.89E-01 m	V_{tube}	431.70 cm^3	Total volume of coolant tubes	m_{tube}	1165.59 g	Total mass of coolant tubes
$s_{Plate\ Act}$	0.63 cm	Actual spacing of plates	0.25 in	6.31E-03 m	V_{fin}	1358.11 cm^3	Total volume of plate fins, including part of fin extruded over the outside of the coolant tubes	m_{fin}	3666.91 g	Total mass of plate fins, including part of fin extruded over the outside of the coolant tubes
m_{bed}	24642.84 g	Mass of bed; including fins, tubes & $NaAlH_4$			V_{gap}	6899.97 cm^3	Total volume of gap including semi-spherical ends	m_{gap}	0.00 g	Total mass of gap including semi-spherical ends
V_{bed}	36237.36 cm^3	Volume of bed with vessel & liner			V_{Liner}	266.38 cm^3	Total volume of liner	m_{Liner}	719.23 g	Total mass of liner
L_{Vessel}	92.64 cm	Overall length of vessel	36.472 in		V_{Tank}	445.52 cm^3	Total volume of tank material	m_{Tank}	668.27 g	Total mass of tank material
					$V_{H2\ inject}$	698.22 cm^3	Total volume of H_2 injection tubes	$m_{H2\ inject}$	565.56 g	Total mass of H_2 injection tubes
Bed Characteristics										
Gravimetric Capacity	0.041 kg H2/Kg Total	With Outer Vessel & Liner			Hydride Grav Capacity	0.056 kg H2/Kg Total	Grav density of $NaAlH_4$ only			
Volumetric Capacity	0.028 kg H2/L Total	With Outer Vessel & Liner			Hydride Vol Capacity	0.040 kg H2/L Total	Vol density of $NaAlH_4$ only			
Radial Distance to Center of Outer Coolant Tubes (Maintains same Area to Cooling Surface Ratio)										
r	8.55 cm	9.50 cm	Radial location of center of coolant tube. Initially guessed, then optimized for hydride area to cooling surface ratio.							
θ	3.04 radians	174.45 °	Angle at center of coolant tube formed by intersection of tube center radius and tube inner wall							
S	2.52 cm		Arc length along inner wall of coolant tube from intersections of tube ceter radius and tube inner wall							
A_1	209.13 cm^2		Cross-sectional area of bed, inside the radius to the center of the coolant tubes, less interior of coolant tubes							
A_2	176.82 cm^2		Cross-sectional area of bed, outside the radius to the center of the coolant tubes, less interior of coolant tubes							
S_1	25.37 cm		Sum of arc lengths of inner wall of all coolnat tubes inside the radius to the center of the cooling tubes							
S_2	21.45 cm		Sum of arc lengths of inner wall of all coolnat tubes outside the radius to the center of the cooling tubes							
Obj Funct	-1.0330E-11		Adjust variable r (the radial location of the center of the coolant tube) to make the objective function zero							

Figure A.1.1 System dimensions calculated with the geometry scoping model.

A.1.2 Heat Removal Scoping Model

Operating parameters for the heat removal system were based on calculations with the Microsoft Excel® heat removal scoping model shown in Figure A.1.2. The system in this report used Dowtherm T® heat transfer fluid for single phase cooling and DuPont Vertrel-XF® heat transfer fluid for two phase cooling. Data sheets, from the respective vendors are listed in Attachments 1 and 2.

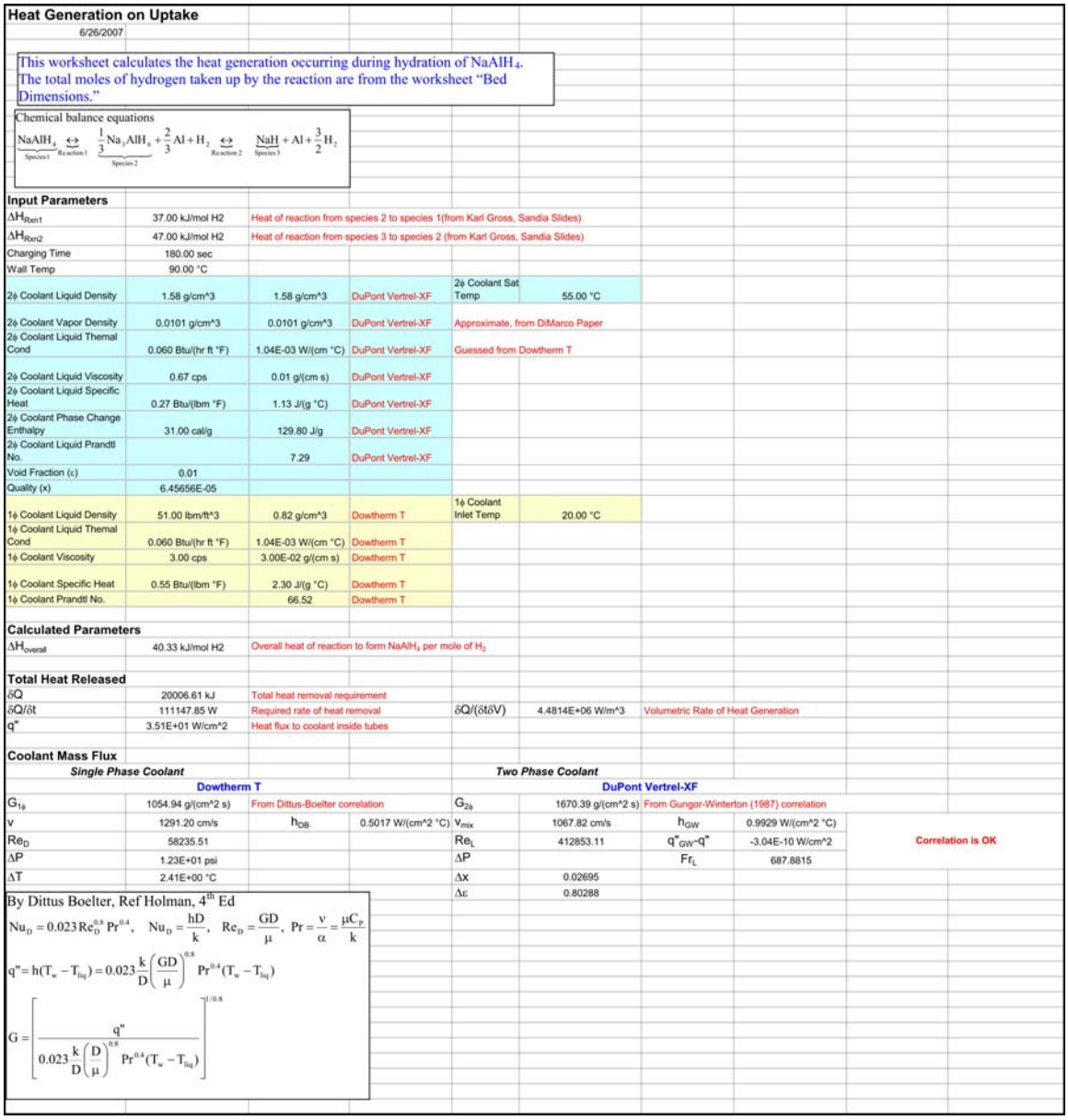

Heat Generation on Uptake

6/26/2007

This worksheet calculates the heat generation occurring during hydration of $NaAlH_4$. The total moles of hydrogen taken up by the reaction are from the worksheet "Bed Dimensions."

Chemical balance equations

$$\underbrace{NaAlH_4}_{\text{Species 1}} \underset{\text{Reaction 1}}{\leftrightarrow} \underbrace{\frac{1}{3}Na_3AlH_6}_{\text{Species 2}} + \frac{2}{3}Al + H_2 \underset{\text{Reaction 2}}{\leftrightarrow} \underbrace{NaH}_{\text{Species 3}} + Al + \frac{3}{2}H_2$$

Input Parameters

ΔH_{Rxn1}	37.00 kJ/mol H2	Heat of reaction from species 2 to species 1(from Karl Gross, Sandia Slides)				
ΔH_{Rxn2}	47.00 kJ/mol H2	Heat of reaction from species 3 to species 2 (from Karl Gross, Sandia Slides)				
Charging Time	180.00 sec					
Wall Temp	90.00 °C					
2ϕ Coolant Liquid Density	1.58 g/cm^3	1.58 g/cm^3	DuPont Vertrel-XF	2ϕ Coolant Sat Temp	55.00 °C	
2ϕ Coolant Vapor Density	0.0101 g/cm^3	0.0101 g/cm^3	DuPont Vertrel-XF	Approximate, from DiMarco Paper		
2ϕ Coolant Liquid Thermal Cond	0.060 Btu/(hr ft °F)	1.04E-03 W/(cm °C)	DuPont Vertrel-XF	Guessed from Dowtherm T		
2ϕ Coolant Liquid Viscosity	0.67 cps	0.01 g/(cm s)	DuPont Vertrel-XF			
2ϕ Coolant Liquid Specific Heat	0.27 Btu/(lbm °F)	1.13 J/(g °C)	DuPont Vertrel-XF			
2ϕ Coolant Phase Change Enthalpy	31.00 cal/g	129.80 J/g	DuPont Vertrel-XF			
2ϕ Coolant Liquid Prandtl No.		7.29	DuPont Vertrel-XF			
Void Fraction (ε)	0.01					
Quality (x)	6.45656E-05					
1ϕ Coolant Liquid Density	51.00 lbm/ft^3	0.82 g/cm^3	Dowtherm T	1ϕ Coolant Inlet Temp	20.00 °C	
1ϕ Coolant Liquid Thermal Cond	0.060 Btu/(hr ft °F)	1.04E-03 W/(cm °C)	Dowtherm T			
1ϕ Coolant Viscosity	3.00 cps	3.00E-02 g/(cm s)	Dowtherm T			
1ϕ Coolant Specific Heat	0.55 Btu/(lbm °F)	2.30 J/(g °C)	Dowtherm T			
1ϕ Coolant Prandtl No.		66.52	Dowtherm T			

Calculated Parameters

$\Delta H_{overall}$	40.33 kJ/mol H2	Overall heat of reaction to form $NaAlH_4$ per mole of H_2				

Total Heat Released

δQ	20006.61 kJ	Total heat removal requirement				
δQ/δt	111147.85 W	Required rate of heat removal		δQ/(δtδV)	4.4814E+06 W/m^3	Volumetric Rate of Heat Generation
q"	3.51E+01 W/cm^2	Heat flux to coolant inside tubes				

Coolant Mass Flux

Single Phase Coolant				*Two Phase Coolant*			
Dowtherm T				DuPont Vertrel-XF			
$G_{1\phi}$	1054.94 g/(cm^2 s)	From Dittus-Boelter correlation		$G_{2\phi}$	1670.39 g/(cm^2 s)	From Gungor-Winterton (1987) correlation	
v	1291.20 cm/s	h_{DB}	0.5017 W/(cm^2 °C)	v_{mix}	1067.82 cm/s	h_{GW}	0.9929 W/(cm^2 °C)
Re_D	58235.51			Re_L	412853.11	$q"_{GW}$-q"	-3.04E-10 W/cm^2
ΔP	1.23E+01 psi			ΔP		Fr_L	687.8815
ΔT	2.41E+00 °C			Δx	0.02695		
				Δε	0.80288		

Correlation is OK

By Dittus Boelter, Ref Holman, 4th Ed

$$Nu_D = 0.023 Re_D^{0.8} Pr^{0.4}, \quad Nu_D = \frac{hD}{k}, \quad Re_D = \frac{GD}{\mu}, \quad Pr = \frac{v}{\alpha} = \frac{\mu C_p}{k}$$

$$q" = h(T_w - T_{liq}) = 0.023 \frac{k}{D}\left(\frac{GD}{\mu}\right)^{0.8} Pr^{0.4}(T_w - T_{liq})$$

$$G = \left[\frac{q"}{0.023 \frac{k}{D}\left(\frac{D}{\mu}\right)^{0.8} Pr^{0.4}(T_w - T_{liq})}\right]^{1/0.8}$$

Figure A.2.2 System heat transfer parameters estimated with the heat removal scoping model.

A.2 KINETICS SCOPING MODEL

A.2.1 $TiCl_3$ Catalyzed $NaAlH_4$ Kinetics

The Mathcad® based UTRC™ kinetics scoping model for $TiCl_3$ catalyzed $NaAlH_4$ is listed in this section of the Appendix. The model can run the reaction of Equation A.2.1-1 in either direction and for any initial composition of $NaAlH_4$, Na_3AlH_6 or NaH. As given by the kinetics, the direction of the reaction depends on the temperature and H_2 pressure. The input parameters for the model below were chosen to cycle the bed.

$$\underbrace{NaAlH_4}_{\text{Species 1}} \underbrace{\leftrightarrow}_{\text{Reaction 1}} \underbrace{\frac{1}{3}Na_3AlH_6}_{\text{Species 2}} + \frac{2}{3}Al + H_2 \underbrace{\leftrightarrow}_{\text{Reaction 2}} \underbrace{NaH}_{\text{Species 3}} + Al + \frac{3}{2}H_2 \qquad \text{A.2.1-1}$$

Evaluation of Kinetics Model for NaH

Reaction

$NaAlH_4 \leftrightarrow 1/3Na_3AlH_6 + 2/3Al + H_2 \leftrightarrow NaH + Al + 3/2H_2$

Species 1 Rxn 1 Species 2 Rxn 2 Species 3

Nomenclature

C_1=Concentration of $NaAlH_4$ (mol/m^3)

C_2=Concentration of Na_3AlH_6 (mol/m^3)

C_3=Concentration of NaH (mol/m^3)

n_{H2}=Moles of H2 taken in to the metal hydride (mol/m^3)

r_{1F}=Rate of formation of $NaAlH_4$ from Na_3AlH_6 (mol/m^3-sec)

r_{1B}=Rate of dissociation of $NaAlH_4$ to Na_3AlH_6 (mol/m^3-sec)

r_{2F}=Rate of formation of Na_3AlH_6 from NaH (mol/m^3-sec)

r_{2B}=Rate of dissociation of Na_3AlH_6 to NaH (mol/m^3-sec)

Note that
$\partial C_2/\partial t = -1/3(\partial C_1/\partial t + \partial C_3/\partial t)$
$\partial n_{H2}/\partial t = \partial C_1/\partial t - 1/2\partial C_3/\partial t$
and
$\partial C_1/\partial t = r_{1F}$ If P>Peq1(T)
$\partial C_1/\partial t = -r_{1B}$ If P<Peq1(T)
$\partial C_3/\partial t = r_{2B}$ If P<Peq1(T)
$\partial C_3/\partial t = -r_{2F}$ If P>Peq1(T)

Tchg := 100

Tdisch := 120

Pchg := 50 Pressure (bar)

Pdisch := 1 Pressure (bar)

General Parameter Values

RR := 8.314 Ideal gas constant (J/mol-K)

Create step function that is 0 or -1 over period 2h

h := 40000 Half Period (sec)

$k(tx) := ceil\left(\frac{tx}{h}\right)$

$test(tx) := 2 \cdot floor\left(\frac{k(tx)}{2}\right) - k(tx)$

$P(tx) := \text{if}(\text{test}(tx) < 0, Pchg, Pdisch)$ Pressure (bar)

Parameter Values (From Fit to Data)

Reaction 1

$A1F := 10^{8}$ $A1B := 4 \cdot 10^{12}$ $\chi 1F := 2.0$ $\chi 1B := 2.0$

$E1F := 80000$ Activation Energy (KJ/mol) $E1B := 110000$ Activation Energy (KJ/mol)

$\Delta H\_R1 := -4475$ $\Delta S\_R1 := -14.83$

Reaction 2

$A2F := 1.5 \cdot 10^{5}$ $A2B := 6 \times 10^{12}$ $\chi 2F := 1.0$ $\chi 2B := 1.0$

$E2F := 70000$ Activation Energy (KJ/mol) $E2B := 110000$ Activation Energy (KJ/mol)

$\Delta H\_R2 := -6150$ $\Delta S\_R2 := -16.22$

Equilibrium Pressure (in bar?)

Reaction 1

$$P\_eq1(TT) := \exp\left(\frac{\Delta H\_R1}{TT + 273} - \Delta S\_R1\right)$$ TT is Temperature in (C)

Reaction 2

$$P\_eq2(TT) := \exp\left(\frac{\Delta H\_R2}{TT + 273} - \Delta S\_R2\right)$$ TT is Temperature in (C)

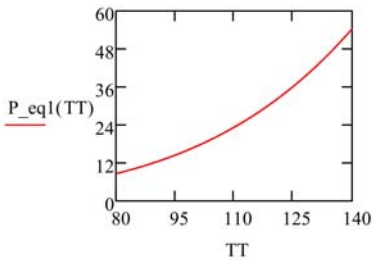

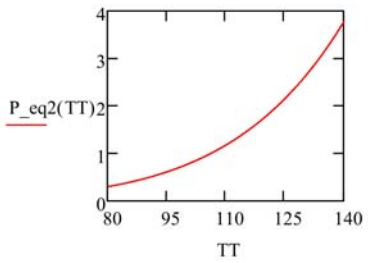

Initial Conditions

$C10 := 0$ $C20 := 0$ $C30 := 330.69$ $nH20 := 0$

$Temp(tx) := \text{if}(\text{test}(tx) < 0, Tchg, Tdisch)$ Temperature (C)

Saturation Concentrations

$Ceqv := C10 + 3 \cdot C20 + C30$ Equivalent Concentration, Needed to relate species concentrations (mol/m^3) to the non-dimensional concenrations used in calculations

Fit the saturation weight fraction to temperature TT is in C

wfdata :=

	0	1
0	300	0.021
1	353	0.021
2	353.15	0.021
3	359	0.022
4	363.15	0.023
5	373.15	0.029
6	393.15	0.022
7	405	0.019
8	413.15	0.018
9	413.5	0.018
10	600	0.018

wfdata := csort(wfdata, 0)

TT is in C

vTT := $\text{wfdata}^{\langle 0 \rangle} - 273.15$

vy := $\text{wfdata}^{\langle 1 \rangle}$

vs := lspline(vTT, vy)

wf_sat(TT) := interp(vs, vTT, vy, TT)

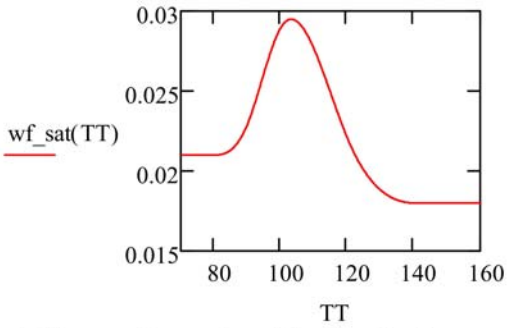

Compute the non-dimensional "saturation" concentrations from fit

$$\text{rsat}(TT) := \max\left(1, 1 - \frac{0.056 - 0.0187}{0.056 - \text{wf\_sat}(TT)}\right)$$ TT is in C

$$\text{C3sat}(TT) := \left(1 - \frac{\text{wf\_sat}(TT)}{0.056}\right) \cdot \text{rsat}(TT)$$ TT is in C

$$\text{C2sat}(TT) := \frac{(1 - \text{rsat}(TT)) \cdot (0.056 - \text{wf\_sat}(TT))}{(0.056 - 0.0187)}$$ TT is in C

Forward and Backward Reaction Rates

$$r1F(TT,tx) := \text{if}\left[(P(tx) \geq P\_eq1(TT)), Ceqv \cdot A1F \cdot \exp\left[\frac{-E1F}{RR\cdot(TT+273.15)}\right]\cdot\frac{P(tx)-P\_eq1(TT)}{P\_eq1(TT)}, 0\right]$$ TT is in C

$$r1B(TT,tx) := \text{if}\left[(P(tx) < P\_eq1(TT)), Ceqv \cdot A1B \cdot \exp\left[\frac{-E1B}{RR\cdot(TT+273.15)}\right]\cdot\left[\frac{(P\_eq1(TT)-P(tx))}{P\_eq1(TT)}\right], 0\right]$$

$$r2F(TT,tx) := \text{if}\left[(P(tx) \geq P\_eq2(TT)), Ceqv \cdot A2F \cdot \exp\left[\frac{-E2F}{RR\cdot(TT+273.15)}\right]\cdot\left[\frac{(P(tx)-P\_eq2(TT))}{P\_eq2(TT)}\right], 0\right]$$

$$r2B(TT,tx) := \text{if}\left[(P(tx) < P\_eq2(TT)), Ceqv \cdot A2B \cdot \exp\left[\frac{-E2B}{RR\cdot(TT+273.15)}\right]\cdot\left(\frac{P\_eq2(TT)-P(tx)}{P\_eq2(TT)}\right), 0\right]$$

Hydrogen Concentration From Kinetics Equations

Given

$$\frac{d}{dt}C1(t) = r1F(Temp(t),t)\cdot\left(\left(\frac{3\,C2(t)}{Ceqv} - C2sat(Temp(t))\right)\right)^{\chi 1F} - r1B(Temp(t),t)\cdot\left(\frac{C1(t)}{Ceqv}\right)^{\chi 1B}$$

$$\frac{d}{dt}C2(t) = -\left[\frac{1}{3}\cdot\left(\frac{d}{dt}C1(t) + \frac{d}{dt}C3(t)\right)\right]$$

$$\frac{d}{dt}C3(t) = -r2F(Temp(t),t)\cdot\left(\frac{C3(t)}{Ceqv} - C3sat(Temp(t))\right)^{\chi 2F} + r2B(Temp(t),t)\cdot\left(\frac{3\,C2(t)}{Ceqv}\right)^{\chi 2B}$$

$$\frac{d}{dt}nH2(t) = \frac{d}{dt}C1(t) - \frac{1}{2}\cdot\left(\frac{d}{dt}C3(t)\right)$$ nH2 is the number of moles of H2 per volume of hydride that are contained for release in the metal hydride

$$C1(0) = C10 \quad C2(0) = C20 \quad C3(0) = C30 \quad nH2(0) = nH20$$

$$\begin{pmatrix} C1 \\ C2 \\ C3 \\ nH2 \end{pmatrix} := Odesolve\left[\begin{pmatrix} C1 \\ C2 \\ C3 \\ nH2 \end{pmatrix}, t, 240000, 20000\right]$$ t is time in seconds

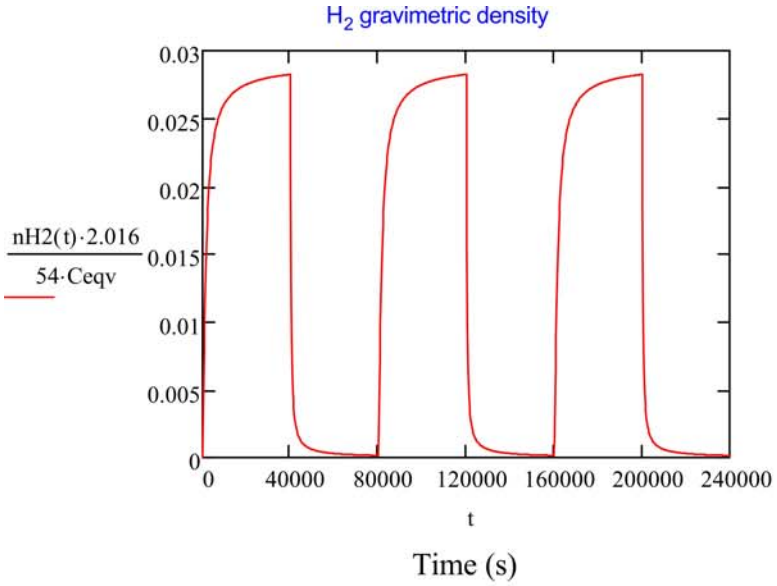

$$\frac{nH2(720)\cdot 2.016}{54\cdot Ceqv} = 0.007940$$

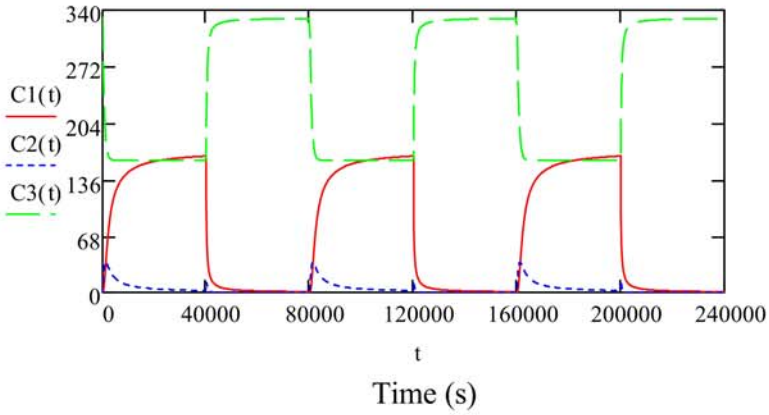

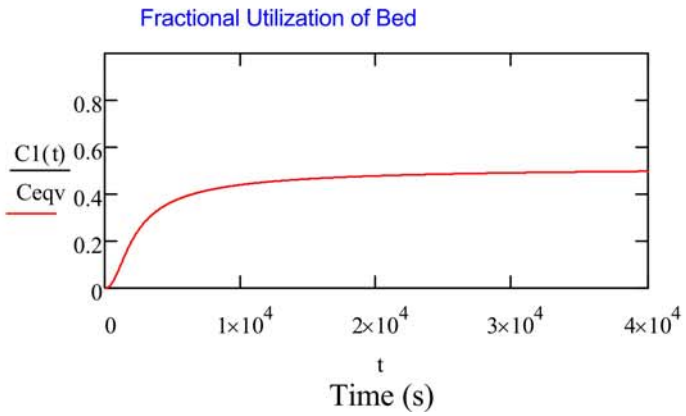

A.2.2 α-ALH_4 Kinetics

The kinetics for α-AlH_4 is based on the correlation of Graetz and Reilly [2005]. The correlation was input to Mathcad® and used to calculate the transient concentration of α-AlH_4 and the release rate of H_2, under discharge conditions for temperatures ranging from 80°C to 120°C. An example of the Mathcad® model, at 110°C, used for these calculations is listed below.

Evaluation of α-AlH_3 Decomposition Kinetics

Nomenclature

C_{α_AlH3}=Concentration of α-phase AlH_3 (mol/m^3)

General Parameter Values

RR := 8.314 Ideal gas constant (J/mol-K)
P := 68 Pressure (bar)

Fit Parameter Values (From Graetz, J. and J. J. Reilly. "Decomposition Kinetics of the AlH_3 Polymorphs." *J. Phys Chem,* B 2005, 109, 22181-22185)

$$A\_AlH3 := 1.2 \cdot 10^{10}$$

E_AlH3 := 102.2 Activation Energy (KJ/mol)

Reaction Rate

$$k(TT) := A\_AlH3 \cdot \exp\left(\frac{-E\_AlH3 \cdot 1000}{RR \cdot TT}\right)$$

ln(k(300)) = −17.767

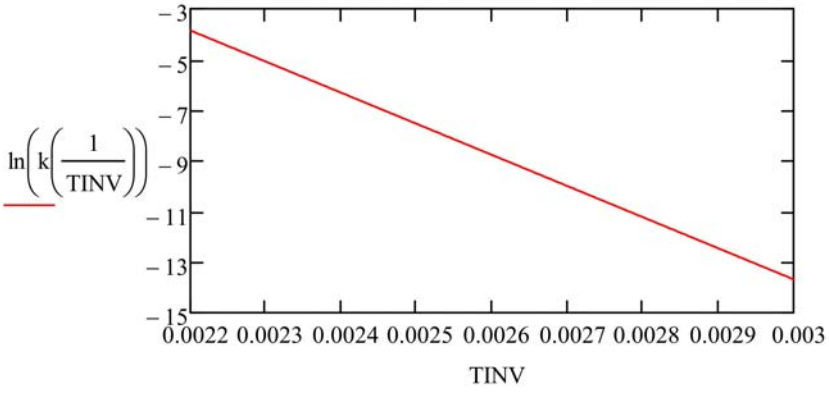

$TempAlane := 110$ AlaneTemperature (C)

$Ca\_AlH30 := 30$ AlaneConcentration (mol/m3)

$$alpha(t, TT) := 1 - \exp\left[-(k(TT + 273.15)\cdot t)^2\right]$$

$$deriv(t, TempAlane) := 2Ca\_AlH30\cdot k(TempAlane + 273.15)^2\cdot t\cdot\exp\left[-(k(TempAlane + 273.15)\, t)^2\right]$$

Alane Concentration From Rate Equations

Given

$$\frac{d}{dt}Ca\_AlH3(t) = if\left[(Ca\_AlH3(t) \geq 0), -Ca\_AlH30\cdot\frac{d}{dt}alpha(t, TempAlane), 0\right]$$

$$Ca\_AlH3(0) = Ca\_AlH30$$

$Ca\_AlH3 := Odesolve(t, 110000, 1000)$

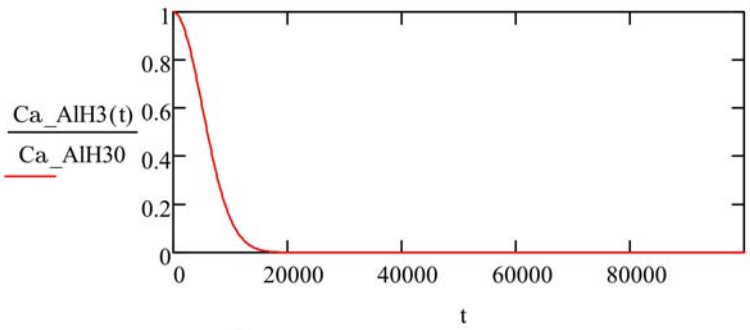

$nH2(tt) := \frac{3}{2}\cdot(Ca\_AlH3(tt) - Ca\_AlH30)$ Moles of H_2 released per m^3 of hydride decomposed

$rate\_nH2(t) := -\frac{3}{2\cdot Ca\_AlH30}\frac{d}{dt}Ca\_AlH3(t)$ Rate of moles of H_2 released per mole of α-AlH_3 decomposed

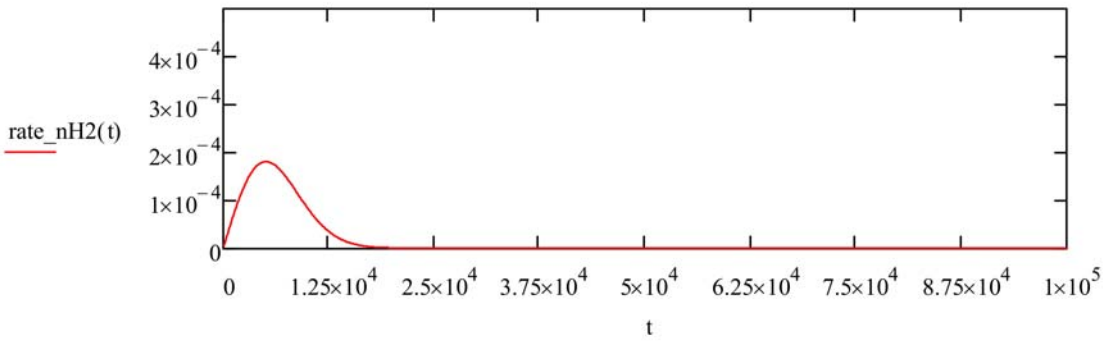

ATTACHMENTS

Att.1 Properties of Dowtherm T®

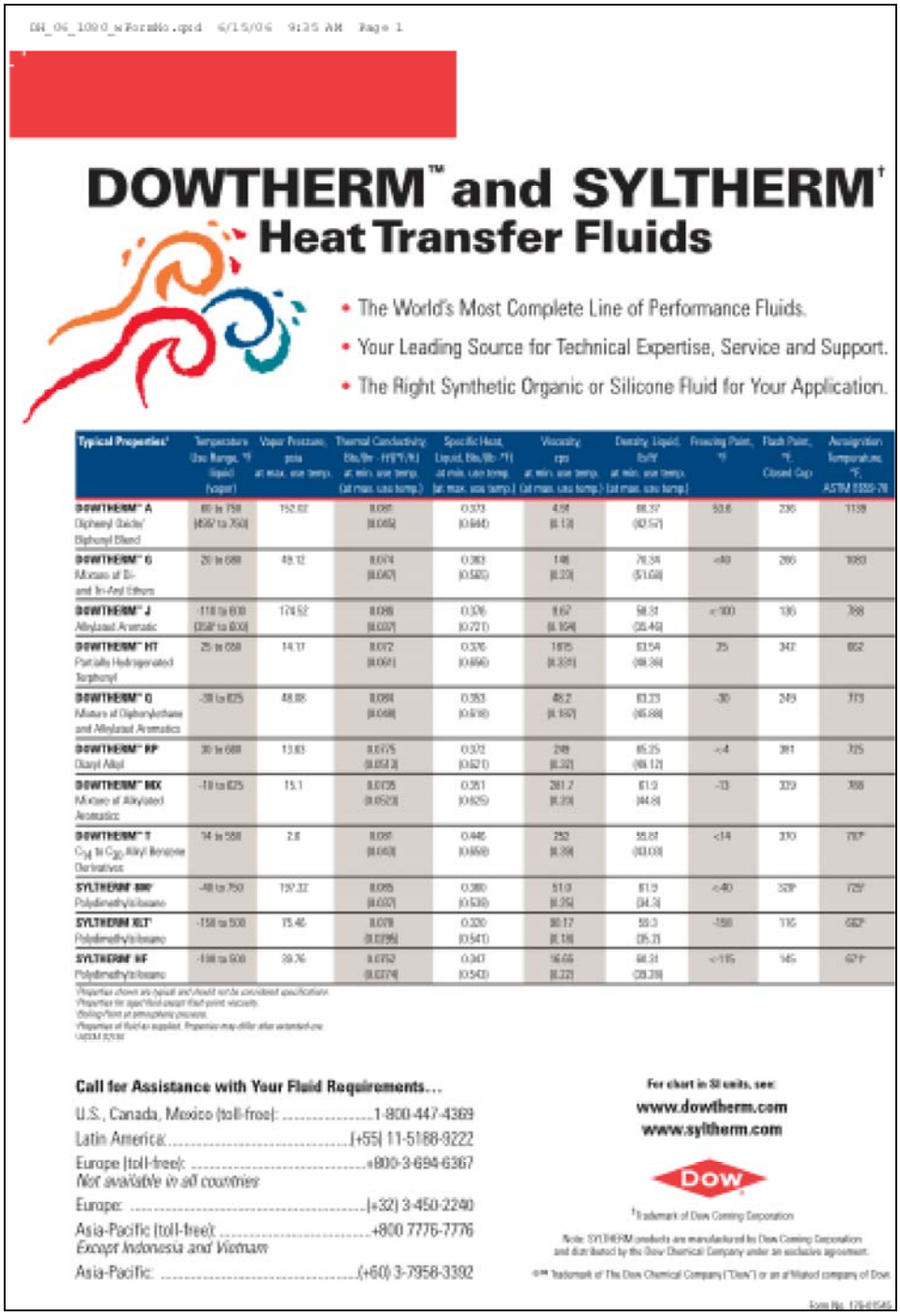

DH_06_1090_wFormlo.qxd 6/15/06 9:25 AM Page 1

DOWTHERM™ and SYLTHERM† Heat Transfer Fluids

- The World's Most Complete Line of Performance Fluids.
- Your Leading Source for Technical Expertise, Service and Support.
- The Right Synthetic Organic or Silicone Fluid for Your Application.

Typical Properties[1]	Temperature Use Range, °F (vapor)	Vapor Pressure, psia at max. use temp.	Thermal Conductivity, Btu/hr · ft[2](°F/ft) at min. use temp. (at max. use temp.)	Specific Heat, Liquid, Btu/lb-°F at min. use temp. (at max. use temp.)	Viscosity, cps at min. use temp. (at max. use temp.)	Density, Liquid, lb/ft³ at min. use temp. (at max. use temp.)	Freezing Point, °F	Flash Point, °F, Closed Cup	Autoignition Temperature, °F, ASTM E659-78
DOWTHERM™ A Diphenyl Oxide/ Biphenyl Blend	80 to 750 (495° to 750)	152.07	0.081 (0.065)	0.373 (0.644)	4.91 (0.13)	66.37 (52.57)	53.6	235	1139
DOWTHERM™ G Mixture of Di- and Tri-Aryl Ethers	20 to 688	48.12	0.074 (0.067)	0.383 (0.585)	1.48 (0.23)	70.34 (51.66)	<40	280	1083
DOWTHERM™ J Alkylated Aromatic	-110 to 600 (350° to 600)	174.52	0.088 (0.077)	0.376 (0.721)	0.67 (0.164)	58.31 (35.45)	<-100	135	788
DOWTHERM™ HT Partially Hydrogenated Terphenyl	25 to 650	14.17	0.072 (0.061)	0.370 (0.666)	1.875 (0.339)	63.54 (48.36)	25	347	852
DOWTHERM™ Q Mixture of Diphenylethane and Alkylated Aromatics	-30 to 625	48.85	0.084 (0.068)	0.353 (0.618)	48.2 (0.167)	63.23 (45.68)	-30	249	713
DOWTHERM™ RP Diaryl Alkyl	30 to 688	13.83	0.0775 (0.0513)	0.372 (0.621)	249 (0.32)	65.25 (48.12)	<-4	381	725
DOWTHERM™ MX Mixture of Alkylated Aromatics	-10 to 625	15.1	0.0735 (0.0520)	0.351 (0.625)	281.7 (0.33)	61.9 (44.8)	-13	329	788
DOWTHERM™ T C_{14} to C_{30} Alkyl Benzene Derivatives	14 to 550	2.8	0.087 (0.063)	0.448 (0.659)	252 (0.39)	55.87 (43.03)	<14	370	797
SYLTHERM 800† Polydimethylsiloxane	-40 to 750	197.32	0.085 (0.072)	0.380 (0.530)	51.0 (0.25)	61.9 (34.3)	<-40	328	729
SYLTHERM XLT† Polydimethylsiloxane	-150 to 500	15.46	0.078 (0.0795)	0.320 (0.547)	30.17 (0.18)	59.3 (35.7)	-150	116	662
SYLTHERM HF Polydimethylsiloxane	-108 to 500	28.76	0.0752 (0.0774)	0.347 (0.543)	16.05 (0.22)	60.31 (28.28)	<-115	145	671

[1]Properties shown are typical and should not be considered specification.
[2]Properties for vapor/liquid except flash point viscosity.
[3]Boiling Point at atmospheric pressure.
[4]Properties of fluid as supplied. Properties may differ after extended use.
[5]ASTM D3701

Call for Assistance with Your Fluid Requirements...

U.S., Canada, Mexico (toll-free): 1-800-447-4369
Latin America: ..... (+55) 11-5188-9222
Europe (toll-free): ..... +800-3-694-6367
Not available in all countries
Europe: ..... (+32) 3-450-2240
Asia-Pacific (toll-free): ..... +800 7776-7776
Except Indonesia and Vietnam
Asia-Pacific: ..... (+60) 3-7958-3392

For chart in SI units, see:
www.dowtherm.com
www.sytherm.com

DOW

†Trademark of Dow Corning Corporation

Note: SYLTHERM products are manufactured by Dow Corning Corporation and distributed by the Dow Chemical Company under an exclusive agreement.

™® Trademark of The Dow Chemical Company ("Dow") or an affiliated company of Dow

Form No. 176-01545

Att.2 Properties of DuPont Vertrel-XF®

Technical Information

DuPont™ Vertrel® XF

Specialty Fluid

Introduction

DuPont™ Vertrel® XF is a proprietary hydrofluorocarbon fluid with "zero" ozone depletion and a low global warming potential ideally suited for use in vapor degreasing equipment for cleaning, rinsing, and drying. It can replace current hydrochlorofluorocarbon (HCFC) and perfluorocarbon (PFC) fluids in most applications.

Vertrel® XF is HFC 43-10mee or 2,3-dihydrodecafluoropentane, empirical formula $C_5H_2F_{10}$. It is a clear, colorless liquid with the properties shown in **Tables 1–2**.

Unique physical properties include a high density, low viscosity, and low surface tension. This combined with nonflammability, chemical and thermal stability, low toxicity, and ease of recovery by distillation make Vertrel® XF ideal for a broad range of applications. Solvency is selective, but can be enhanced by use of appropriate azeotropes and blends with alcohols, hydrocarbons, esters, etc. (see **Table 3**).

Table 1
Physical Properties

Property*	Vertrel® XF
Molecular Weight	252
Boiling Point, °C (°F)	55 (130)
Vapor Pressure, mmHg (psia)	228 (4.4)
Freezing Point, °C (°F)	-80 (-112)
Liquid Density, g/cc (lb/gal)	1.58 (13.2)
Surface Tension, dyn/cm	14.1
Viscosity, cPs	0.87
Solubility in Water, ppm	140
of Water, ppm	480
Critical Temperature, °C (°F)	178 (353)
Critical Pressure, psia (atm)	339.9 (22.8)
Critical Volume, cc/mol	433
Heat of Vaporization (at boiling point), cal/g (Btu/lb)	31.0 (55.7)
Specific Heat, cal/g/°C (Btu/lb/°F)	0.27 (0.27)
Dielectric Constant	7-10
Breakdown Voltage, kV	
Liquid	14-28
Vapor	10-12
Volume Resistivity, ohm-cm	10^{9} – 10^{11}
Flash Point	
Closed Cup	None
Open Cup	None
Flammable Range, Air	None

* At 25°C (77°F) except where indicated.
† Pensky-Martens Closed Cup Tester (ASTM D93)
‡ Tag Open Cup Tester (ASTM D1310)

Typical Applications

- Cleaning and rinsing agent
- Drying fluid
- Particulate remover
- Fluorocarbon lubricant carrier
- Solvent and dispersion media
- Heat transfer media
- Dielectric fluid
- Replacement for many HCFC, PFC, and CFC-113 applications

Vertrel® XF is ideally suited for cleaning fine particulate matter (submicron range) from metal and nonmetal parts. Removal of particle contamination requires a solvent that can minimize the thickness of the laminar boundary layer where particles are bonded to the substrate. If the boundary layer thickness is less than the particle diameter, momentum from the flowing solvent can efficiently dislodge the particles and carry them away. Vertrel® XF, with its lower viscosity and higher density, results in a thinner boundary layer, which enhances cleaning. Common aqueous cleaning fluids, mixtures of water and detergent, have higher viscosities and lower densities compared to Vertrel® XF, making these fluids less efficient.

The electronic attraction between particle and surface can be overcome further by increasing the polarity of the fluid through the addition of small amounts of alcohols. DuPont offers a series of proprietary azeotrope and blend compositions which exploit this property (see **Table 3**).

Another common cleaning technique is the addition of ultrasonics to the solvent. High frequency, ultrasonic waves produce tiny bubbles which form and collapse (cavitate) as the wave passes. Cavitation energy increases with decreasing viscosity, another advantage of Vertrel® XF, improving its ability to mechanically dislodge particle contamination.

Vapor Degreasing Process

Use of modern vapor containment technology is recommended for both batch and in-line equipment. These systems have higher freeboard and a secondary set of low-temperature (–29°C [–20°F]) condenser coils to greatly reduce vapor losses from boiling solvent degreasing, defluxing, rinsing, and drying equipment.

Neat Vertrel® XF can be used for rinsing, drying, and some cleaning applications, but use with other components, such as azeotropes or simple blends, can provide improved solvency and soil removal. Vertrel® XF forms azeotropes or constant boiling mixtures with many similar boiling range components. Five nonflammable proprietary azeotrope compositions have been developed that are useful for general and precision cleaning and defluxing. See specific product bulletins for details.

DUPONT

The miracles of science™

Table 2
Density and Vapor Pressure Change with Temperature

Temperature, °C (°F)	Density, g/cc (lb/g)	Vapor Pressure, mmHg (psia)
–20 (–4)	1.70 (14.2)	18 (0.3)
–10 (14)	1.68 (14.0)	36 (0.7)
0 (32)	1.66 (13.8)	62 (1.2)
10 (50)	1.62 (13.5)	109 (2.1)
20 (68)	1.60 (13.3)	178 (3.4)
30 (86)	1.57 (13.1)	284 (5.5)
40 (104)	1.55 (12.9)	434 (8.4)
50 (122)	1.51 (12.6)	641 (12.4)
60 (140)	1.49 (12.4)	921 (17.8)
70 (158)	1.46 (12.2)	1288 (24.9)
80 (176)	1.43 (11.9)	1753 (33.9)
90 (194)	1.40 (11.7)	2343 (45.3)
100 (212)	1.38 (11.5)	3072 (59.4)
110 (230)	1.34 (11.2)	3981 (76.6)
120 (248)	1.32 (11.0)	5083 (97.3)
130 (266)	1.30 (10.8)	6309 (122.0)

Table 3
Azeotropes of Vertrel® XF

Product	Vertrel® XF With	Boiling Point, °C (°F)
Vertrel® XM	Methanol	46(115)
Vertrel® XE	Ethanol	52(126)
Vertrel® XP	Isopropanol	52(126)
Vertrel® MCA	Trans-1,2-Dichloroethylene	39(102)
SMT	Trans-1,2-Dichloroethylene and Methanol	37(99)

Co-solvent Process

The co-solvent process is a cleaning process that uses a high-boiling, low-volatility solvating agent in combination with Vertrel® XF, in a two-sump vapor degreaser. Parts are immersed into the boil sump containing the solvating agent blended with Vertrel® XF. Parts are then held over the boil sump and optionally sprayed to remove loose contaminants and the solvating agent. The rinse sump contains only Vertrel® XF. Parts are immersed in the rinse sump with optional ultrasonics where final traces of soil and solvating agent are removed. The parts are then held in the vapor zone to complete the drying cycle.

Vertrel® XF is ideally suited for the co-solvent process, because the typical solvating agents are partially to completely miscible with Vertrel® XF, greatly improving the overall cleaning and rinsing efficiency. **Table 4** is a partial list of typical solvating agents. Where the solvating agent is flammable, use of a co-solvent system ameliorates the flammability hazard by providing an inert vapor blanket.

Solvency

Unlike the PFCs, Vertrel® XF is completely miscible with most esters, ketones, ethers, ether-alcohols, and the lower alcohols, such as methanol, ethanol, and isopropanol. The lower hydrocarbons, such as hexane and heptane, are also soluble. Neat Vertrel® XF has limited solvency for many higher molecular weight materials, such as hydrocarbon oils, silicone oils, waxes, and greases; here combinations with the many readily miscible esters, alcohols, and lower hydrocarbons can enhance solubility and cleaning efficiency. Like CFC-113 and the PFCs, Vertrel® XF has high solubility for Krytox® and "Fomblin" fluorocarbon lubricants and can be used either as an application carrier fluid or to remove them.

Table 4
Vertrel® XF Solvating Agents

Dibasic Esters (DBE)	Aliphatic Alcohols
Aliphatic Hydrocarbons	Methyl Decanoate
Propylene Glycol N-Propyl	Dibutyl DBE
N-Methyl-2-Pyrrolidone (NMP)	Isopropyl Myristate
Dipropylene Glycol Butyl Ether	
Dipropylene Glycol Monomethylether	
Tetrahydrofurfuryl Alcohol (THFA)	

Plastic and Elastomer Compatibility

A large variety of plastics and elastomers can be safely exposed to Vertrel® XF. **Tables 5 and 6** summarize test results on short-term exposures of unstressed plastics and elastomers which simulate a typical cleaning cycle.

Long-term compatibility data simulating exposure of vapor degreaser construction materials is available from DuPont upon request.

Elastomer swelling and shrinking will, in most cases, revert to within a few percent of original size after air drying. Swell, shrinkage, and extractables are strongly affected by the compounding agents, plasticizers, and curing used in the manufacture of plastics and elastomers. Therefore, prior in-use testing is particularly important.

Table 5
Plastic Compatibility
Immersion: 15 Minutes at Room Temperature

Compatible	
Polyethylene	ABS
Polypropylene	Acetal
Polystyrene	Epoxy
Polyester, PET, PBT	Ionomer
Polyphenylene Oxide, PPO	Liquid Crystal Polymer
Polyimide, PI, PEI, PAI	Phenolic
Polyetherketone, PEK	PVC, CPVC
Polyaryletherketone, PEEK	PTFE, ETFE
Polysulfone	
Polyarylsulfone	
Polyphenylene Sulfide, PPS	

Incompatible*	
Acrylic	Cellulosic

*Material composition varies depending upon compounding agents, plasticizers, processing, etc. Specific materials should be tested for compatibility with solvent.

Table 6
Elastomer Compatibility
Immersion: 15 Minutes at Room Temperature

Compatible	
Buna N, NBR, Nitrile	Buna S, SBR, GRS
Butyl Rubber, IIR	Chlorosulfonated PE
EPM, EPDM, Nordel®	Polysulfide
Natural Rubber, Isoprene	Neoprene
Urethane	Viton® B
	Silicone
Incompatible*	
None Tested	

*Materials composition varies depending upon compounding agents, plasticizers, processing, etc. Specific material should be tested for compatibility with solvent.

Metals and Other Compatibility

Vertrel® XF is fully compatible with the metals listed below after exposure for two weeks at 100°C (212°F) in sealed tubes with and without water contact.

- Zinc*
- Aluminum
- Stainless Steel
- Copper*
- Brass*

Vertrel® XF is not compatible with strong bases; therefore, contact with highly basic process materials is not recommended.

*Slight discoloration with water present

Exposure Limits

Data from acute toxicity studies has demonstrated that Vertrel® XF has low toxicity. Vertrel® XF is a slight skin and eye irritant and has low acute inhalation toxicity. **Table 7** shows the applicable exposure limits for Vertrel® XF.

Table 7
Exposure Limits

Component	Limit, p pm	Type
Vertrel® XF	AEL* 200 400	8- and 12-hr TWA Ceiling*

*AEL (Acceptable Exposure Limit) is an airborne inhalation exposure limit established by DuPont that specifies time-weighted average concentrations to which nearly all workers may be repeatedly exposed without adverse effects.

*A ceiling limit is the concentration that should not be exceeded during any part of the working day. The ceiling limit for individual components applies to a blend product as well.

Safety/Flammability

Vertrel® XF is nonflammable and does not become flammable during boiling or evaporation. It exhibits no closed or open cup flash point, and is not classified as a flammable liquid by NFPA or DOT. It is thermally stable to 300°C (572°F) and does not oxidize or degrade during storage.

Recovery

Vertrel® XF is a pure component material, and is easily recoverable by off-line and in-line distillation equipment such as a vapor degreaser or still. The presence of soil, however, may alter the characteristics of the material during the recovery operation. Recovery should be closely monitored to ensure operating levels are maintained. Users should test the spent Vertrel® XF to ensure proper classification for waste disposal.

Storage/Handling

Vertrel® XF is thermally stable and does not oxidize or degrade during storage. Store in a clean, dry area. Protect from freezing temperatures. Do not allow stored product to exceed 52°C (125°F) to prevent leakage or potential rupture of container from pressure and expansion.

Consideration should be given to retrofit of existing, or purchase of new, vapor degreasing equipment to provide vapor containment technology that enables safe and economical use of Vertrel® XF.

Drum pumps are recommended to dispense Vertrel® XF from its container. Refer to the Material Safety Data Sheet for specific handling precautions and instructions.

Environmental Legislation

Vertrel® XF has "zero" ozone depletion potential and a low global warming potential (**Table 8**). Vertrel® XF and its azeotropes and blends are used as alternatives to CFC-113, methylchloroform, hydrochlorofluorocarbons (HCFCs), and perfluorocarbons (PFCs) in many critical cleaning, drying, carrier fluid, and other high-value specialty uses where chemical stability is paramount.

Vertrel® XF is accepted by the U.S. Environmental Protection Agency (EPA) under the Significant New Alternatives Policy (SNAP) program as a substitute for ozone-depleting substances. HFC 43-10mee or decafluoropentane is exempt from classification as a volatile organic compound (VOC) by the EPA. Vertrel® XF is also VOC compliant under the California South Coast Air Quality Management District (SCAQMD) regulations, which require VOC content less than 50 g/L of solvent.

Vertrel® XF is listed in the TSCA inventory. It is subject to the Significant New Use Rule (SNUR) and should be used only in the indicated applications. See MSDS Regulatory Section.

Vertrel® XF is not a hazardous air pollutant (HAP), and therefore not subject to NESHAP regulation. Spent Vertrel® XF is not a RCRA characteristic or listed waste. However, addition of contaminants could change that status. Vertrel® XF is not included in the SARA Title III Section 313 list of toxic chemicals, and is not subject to SARA Title III (EPCRA) reporting requirements.

Packaging and Availability

Vertrel® XF is commercially available in 55-gal (208-L) drums with a net weight of 660 lb (299 kg) and in 5-gal (20-L) pails with a net weight of 60 lb (27 kg). One-gallon and smaller samples in glass containers are available on request. Customers are encouraged to secure samples now for compatibility and performance testing.

Specifications

Composition and specifications are shown in **Table 9**. Vertrel® XF is listed in the TSCA Inventory.

Table 8
Environmental Properties

Property	Vertrel® XF
Formula	$C_5H_2F_{10}$
Class	Hydrofluorocarbon (HFC)
Atmospheric Lifetime, yr	17.1
Ozone-Depletion Potential (ODP)	0
Global Warming Potential (GWP/100 yr ITH)	1300
Volatile Organic Compounds (VOC; g/L)	Exempt

Table 9
Vertrel® XF Specifications

Fluoropentanes, wt%	99.9 min.
Nonvolatile Residue, ppm wt	2.0 max.
Moisture, ppm wt	50 max.
Acidity, mg KOH/g	0.01 max.
Appearance	Clear, Colorless

North America, Canada, Mexico
Micro Care Marketing Services
595 John Downey Drive
New Britain, CT 06051
Tel: (888) 595-4525
Fax: (860) 827-8105

Europe, Africa, Middle East
DuPont de Nemours
International S.A.
2 Chemin du Pavillon
P.O. Box 50
CH-1218 Le Grand-Saconnex
Geneva, Switzerland
41-22-717-51 11

South America
DuPont do Brasil S.A.
Alameda Itapecuru, 506
Alphaville 06454-080 Barueri
Sao Paulo, Brasil
55-11-7266-8263

Pacific
DuPont Australia
P.O. Box 930
North Sydney, NSW
Australia 2060
61-2-923-6165

Japan
DuPont-Mitsui
Fluorochemicals
Co., Ltd.
Chiyoda Honshu Bldg.
5-18 Sanguku-cho 1-Chome
Chiyoda-Ku, Tokyo 101,
Japan
(03) 5281-5805

Asia
DuPont Taiwan
P.O. Box 81-777
Taipei, Taiwan
886-2-514-4400

DuPont Asia Pacific, Ltd.
P.O. Box TST 98851
Tsim Sha Tsui
Kowloon, Hong Kong
852-734-5345

DuPont Thailand
G.P.O. Box 2598
Bangkok 10500, Thailand
66-2-236-0026

DuPont Far East, Inc.
8/F Solid Bank Bldg.
777 Paseo de Roxas
Makati 1226 Philippines
63-2-818-0911

DuPont Far East Inc.
P.O. Box 7882
40702 Shah Alam, Malaysia
60-3-519-3006

DuPont Korea Ltd.
C.P.O. Box 5972
Seoul, Korea
82-2-721-5114

DuPont Singapore Pte. Ltd.
1 Maritime Square #07-01
World Trade Centre
Singapore 0409
65-273-2244

[illegible] Printed in U.S.A.
[illegible]
[illegible]

DUPONT
The miracles of science™

Att.3 UTRC™ Sodium Alanate Kinetics 1

Practical Sorption Kinetics of $TiCl_3$ Catalyzed $NaAlH_4$

Xia Tang, Daniel A Mosher and Donald L Anton

United Technologies Research Center

411 Silver Lane

East Hartford, CT 06108

Abstract

Sodium alanate has been studied as a promising candidate material for reversible hydrogen storage due to its intermediate temperature range and relatively high storage capacity. Its rates of desorption and absorption of hydrogen have been shown to be enhanced by the addition of Ti in various compounds. To date, the sorption kinetics, especially absorption kinetics, is not well understood. In this study, a practical sorption kinetics model for $TiCl_3$ catalyzed $NaAlH_4$ has been developed to assist in the engineering design and evaluation of a prototype hydrogen storage system.

Introduction

The design of a hydrogen storage system using any exothermic hydriding compound, such as $NaAlH_4$, requires detailed consideration of local heat management. This is especially important in the critical hydrogen absorption stage, where high kinetics are required and heat flow is at its maximum. Thermal transport architectures such as cooling tubes and metal foam structures need to be designed to meet the optimum operational characteristics of the hydrogen storage media. In order to design and model these architectures and obtain a gravimetrically and volumetrically optimized storage system, absorption and desorption kinetic models need to be identified and validated. Many current models, such as the well-known Arrhenius model, are insufficient to characterize materials behavior under transient or partially discharged conditions. Previous kinetics studies of $NaAlH_4$ mainly focused on the desorption reaction [1-4]. Aborption and desorption kinetics models were developed by Luo and Cross [5] to simulate NaH+Al $\leftrightarrow$$NaAlH_4$ reactions using NaH and Al as starting materials. No kinetics model was reported to simulate transient hydriding rate and hydrogen absorption capacity of NaH+Al derived from $NaAlH_4$. In this study, a solid/gas chemical kinetics model originally developed by El-Osery [6-9] to design conventional metal hydride systems was utilized. This model was adapted for use in the multi-step hydrogen absorption mechanisms of NaH+Al$\rightarrow$$NaAlH_4$.

Basic Kinetics Model

The dehydrogenation and hydrogenation of sodium alanate involve the following well-known reactions:

$NaAlH_4 \leftrightarrow 1/3\ Na_3AlH_6 + 2/3\ Al + H_2 \leftrightarrow\ NaH + Al + 3/2\ H_2$

For compactness, the compositional state can be tracked by a single variable for each product/reactant, C_1, C_2 and C_3 as:

C_1: $NaH + Al + 3/2\ H_2$

C_2: $1/3\ Na_3AlH_6 + 2/3\ Al + H_2$

C_3: $NaAlH_4$

The nomenclatures for all reactions are listed in Table 1.

Table 1 Nomenclature for All Reactions

Label	Action	Reactant	Product
r_1	Dehydriding of Na_3AlH_6	C_2	C_1
r_2	Hydriding of NaH	C_1	C_2
r_3	Dehydriding of $NaAlH_4$	C_3	C_2
r_4	Hydriding of Na_3AlH_6	C_2	C_3

Reaction rates can be represented by equation (1) based on the metal hydride model developed by El-Osery [6-7]:

$$\left(\frac{dC_j}{dt}\right)_{r_i} = f_T(T) * f_P(P) * f_C(C_k) \quad (1)$$

i for reaction r_i
j for composition product C_j
k for composition reactant C_k.

The temperature dependant term is that of the typical Arrhenius equation given as:

$$f_T = A_i \exp\left(-\frac{E_i}{RT}\right) \quad (1a)$$

The pressure dependant term can be expressed simply as a first order expression:

$$f_P = (-1)^i * \left(\frac{P - P_{e,i}}{P_{e,i}}\right) \quad (1b)$$

where $P_{e,i}$ is the equilibrium pressure for the reaction and is valid for both hydriding and dehydriding. Equilibrium pressure $P_{e,i}$ is temperature dependant and obeys the van't Hoff equation:

$$\ln(P_{e,i}) = \frac{\Delta H}{RT} - \frac{\Delta S}{R} \quad (1c)$$

In El-Osery's description, a first order function of hydrogen/metal atomic ratio was used in a concentration factor for hydriding. In hydriding reactions of the NaH+Al system, however, two solid reactants are involved in each reaction respectively. They may have higher reaction orders. The concentration factor is thus represented as being proportional to the reactant concentration to some power, χ_i as:

$$f_C = (C_k)^{\chi_i} \quad (1d)$$

Combining these factors results in the rate equation:

$$\frac{dC_j}{dt} = A_i \exp\left(-\frac{E_i}{RT}\right) * (-1)^i * \left(\frac{P - P_{e,i}}{P_{e,i}}\right) * (C_k)^{\chi_i} \quad (2)$$

Applying equation (2) to r_2 and r_4, one obtains the following equations for high pressure hydriding (r_2 and r_4 are active).

$$\left(\frac{dC_2}{dt}\right)_{r2} = A_2 \exp\left(-\frac{E_2}{RT}\right) * \left(\frac{P - P_{e,2}}{P_{e,2}}\right) * (C_1)^{\chi_2} \text{ and } \left(\frac{dC_1}{dt}\right)_{r2} = -\left(\frac{dC_2}{dt}\right)_{r2}$$

$$\left(\frac{dC_3}{dt}\right)_{r4} = A_4 \exp\left(-\frac{E_4}{RT}\right) * \left(\frac{P - P_{e,4}}{P_{e,4}}\right) * (C_2)^{\chi_4} \text{ and } \left(\frac{dC_2}{dt}\right)_{r4} = -\left(\frac{dC_3}{dt}\right)_{r4}$$

The reaction rate of each composition can be represented as:

$$\frac{dC_1}{dt} = -A_2 \exp\left(-\frac{E_2}{RT}\right) * \left(\frac{P - P_{e,2}}{P_{e,2}}\right) * (C_1)^{\chi_2} \quad (5)$$

$$\frac{dC_2}{dt} = A_2 \exp\left(-\frac{E_2}{RT}\right) * \left(\frac{P - P_{e,2}}{P_{e,2}}\right) * (C_1)^{\chi_2} - A_4 \exp\left(-\frac{E_4}{RT}\right) * \left(\frac{P - P_{e,4}}{P_{e,4}}\right) * (C_2)^{\chi_4} \quad (6)$$

$$\frac{dC_3}{dt} = A_4 \exp\left(-\frac{E_4}{RT}\right) * \left(\frac{P - P_{e,4}}{P_{e,4}}\right) * (C_2)^{\chi_4} \quad (7)$$

$$0 \le C_i \le 1$$

with the initial reaction conditions: $C_1^{t=0} = 1$, $C_2^{t=0} = 0$, $C_3^{t=0} = 0$,

Experimental Procedure

To validate the applicability of this kinetic model, a well-known alanate composition was chosen for empirical assessment. Commercial grade $NaAlH_4$ was purchased from Albemarle Co. (Baton Rouge, LA) with a chemical certification analysis of 86.3% $NaAlH_4$, 4.7%Na_3AlH_6, 7.5% free Al and 10.1% insoluble Al (with all analyses given in wt%). The catalyst, $TiCl_3$ (99.99%), was obtained from Aldrich Corp. All materials were used in the as-received condition.

The $NaAlH_4$ was catalyzed with 4 mol % $TiCl_3$ by high energy SPEX ball milling for three hours under nitrogen. Immediately after ball milling, approximately 1 g of the sample was transferred into the sample holder of a modified Sievert's apparatus. All the storage and transferring of $NaAlH_4$ and $TiCl_3$ were performed under a high purity nitrogen environment inside a glove box with an oxygen concentration $<10^{-5}$ ppm.

$TiCl_3$ catalyzed $NaAlH_4$ was first desorbed at 150°C in vacuum for more than 7 hours to ensure maximum desorption. Absorption was conducted with the hydrogen pressure ranging from 6.8-6.0 MPa. Extent of reaction versus time was measured by monitoring hydrogen pressure change using a gas reaction controller made by Advanced Materials Co. (Pittsburg, PA).

Results and Discussion

Rate equations (5) to (7) represent an ideal kinetics model, where the total charging capacity over long periods approaches the ideal capacity of 5.6 wt%. However, in reality, the total capacity is usually less than the theoretical value. Saturation compositions, $C_k^{Sat}(T)$, are introduced into the rate equations to reflect this non-ideal capacity. They represent the residual reactant compositions at the hydriding saturation point fordifferent temperature values.

The concentration factors in equation (1d) are thus changed to:

$$f_C = \left(C_k - C_k^{sat}(t)\right)^{\chi_i} \text{ if } C_k - C_k^{sat}(T) \ge 0 \quad (1e)$$

$$f_C = 0 \text{ if } C_k - C_k^{sat}(T) < 0 \quad (1f)$$

The rate equations are represented accordingly by:

$$\frac{dC_1}{dt} = -A_2 \exp\left(-\frac{E_2}{RT}\right) * \left(\frac{P - P_{e,2}}{P_{e,2}}\right) * \left[C_1 - C_1^{sat}(T)\right]^{\chi_2} \quad (8)$$

$$\frac{dC_2}{dt} = A_2 \exp\left(-\frac{E_2}{RT}\right) * \left(\frac{P - P_{e,2}}{P_{e,2}}\right) * \left[C_1 - C_1^{sat}(T)\right]^{\chi_2} - A_4 \exp\left(-\frac{E_4}{RT}\right) * \left(\frac{P - P_{e,4}}{P_{e,4}}\right) * \left[C_2 - C_2^{sat}(T)\right]^{\chi_4} \quad (9)$$

$$\frac{dC_3}{dt} = A_4 \exp\left(-\frac{E_4}{RT}\right) * \left(\frac{P - P_{e,4}}{P_{e,4}}\right) * \left[C_2 - C_2^{sat}(T)\right]^{\chi_4} \quad (10)$$

The modified compositions and total hydriding capacity at saturation are:

$$C_1 = C_1^{sat}(T), \quad C_2 = C_2^{sat}(T), \quad C_3 = 1 - C_1^{sat}(T) - C_2^{sat}(T)$$

The total H_2 absorption capacity $w_{iso}^{sat}(T)$:

$$w_{iso}^{sat}(T) = 0.0187 * C_2^{sat}(T) + 0.056 * \left(1 - C_1^{sat}(T) - C_2^{sat}(T)\right) \quad (11)$$

Curve fitting with experimental data using equations (8) to (13) is shown in Figure 1. The parameters used for fitting are listed in Table 2. The slope and intercept in the van't Hoff plot were derived from data published by Cross *et al.* [10].

Table 2 Fitting Parameters in Figure 1

$(\Delta H/R)r_2$	-6150	Slope in van't Hoff plot
$-(\Delta S/R)r_2$	16.22	Intercept in van't Hoff plot
A_2	1.50E+05	Pre-exponent coefficient for r_2
E_2	70	Activation energy for r_2, KJ/mol of H_2 for r_2
χ_2	1	Reaction order for r_2
$(\Delta H/R)r_4$	-4475	Slope in van't Hoff plot, r_4
$-(\Delta S/R)r_4$	14.83	Intercept in van't Hoff plot, r_4
A_4	1.00E+08	Pre-exponent coefficient for r_4
E_4	80	Activation energy for r_2, kJ/mol of H_2 for r_4
χ_4	2	Reaction order for r_4

The activation energies, E_i, for r_2 and r_4 are 70 and 80 KJ/mol of H_2 and the pre-exponent coefficients, A_i, 1.50E+05 and 1.00E+08 respectively. The hydriding reaction, r_4 (Na_3AlH_6 to $NaAlH_4$) has a higher activation energy than the reaction, r_2, NaH to Na_3AlH_6. However, the pre-exponential coefficient of r_4 is much higher than r_2. This could be due to catalyst placement preferentially at positions favorable to r_4 reaction. The reaction orders of the two hydriding steps appear to be different, with r_2 being nominally a first order reaction, and r_4 a second order reaction. The reaction orders are consistent with those reported by Luo and Gross [5]. During the formation of Na_3AlH_6, NaH is the limiting reactant and Al is in access. Al concentration can be considered as constant and the reaction becomes a pseudo first order. In r_4, the reactants, Na_3AlH_6 and Al, are in stichometric ratio. Both concentrations can affect reaction rate. The formation of $NaAlH_4$, therefore, is a second order reaction.

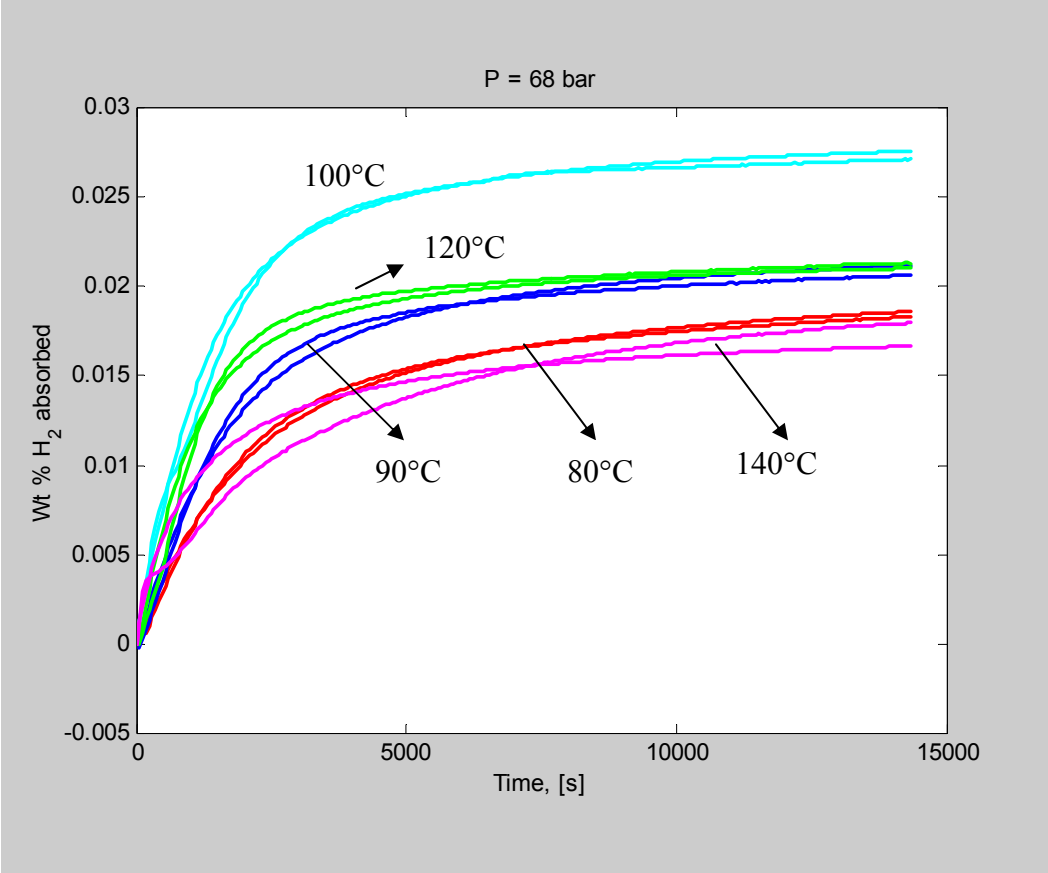

Figure 1 H_2 absorption curves at 80-140°C with H_2 pressure ranging from 6.0-6.8MPa. The dashed lines are model results, with red=80°C; blue=90°C; cyan=100°C; green=120°C; and magenta=140°C.

As shown in Figure 1, the model fits experimental data well in absorption temperature range of 80°C-120°C. However, the fit is not as accurate for absorption at 140°C. As the temperature increases, the hydriding reaction of Na_3AlH_6 to $NaAlH_4$ approaches its thermodynamic equilibrium at 6.0-6.8 MPa hydrogen pressure. The P_e for 2 mol.% $Ti(OBu^n)_4$ catalyzed materials is 5.4 MPa [9]. Although the reaction rate increases with temperature, the capacity decreases as a result of decreasing thermodynamic driving force. Absorption at this temperature is not recommended at this hydriding pressure.

By close inspection. it can be seen in Figure 1 that inflection regions are present during the initial rapid hydriding. Similar inflections were also observed in previous absorption data published by Sandrock *et al.* [11]. There are two possibilities for this observation; (i) a temperature rise in the sample upon exothermic hydriding of NaH to form Na_3AlH_6 or (ii) the combination of slowing down of the first hydriding reaction, r_2, and starting of the second reaction, r_4. To resolve this question, accurate sample temperature measurement is required. This non-isothermal factor can be included in future models when accurate *in-situ* measurement of the sample temperature becomes available. In addition, the current model is fit to isothermal hydriding data, with the assumption that the hydriding rate is not affected by thermal histories except that captured by the variables C_k. Reactions involving solid reactants and products usually involve product nucleation and growth periods, and reaction rates are closely related to the characteristics of these periods. Previous thermal histories could affect particle sizes, packing and reactant/catalyst distribution. These changes will have an effect on the characteristics of nucleation and growth, therefore altering reaction rates. Future kinetics models should take these factors into consideration.

Conclusion

A practical kinetics model has been developed to simulate hydrogen absorption of NaH + Al obtained from $TiCl_3$ catalyzed $NaAlH_4$. Physical meaning of the basic model is discussed. Modification of the model has been made with additional parameters for non-stoichiometric saturation compositions. The modified model fits well with experimental data at temperatures ranging from 80°C to120°C in the pressures range 6.0-6.8MPa. This model has provided kinetic information needed in the design of 1 kg hydrogen storage system using $NaAlH_4$ as storage media. Although this model needs further refinement to include non-isothermal factors and solid state reaction mechanisms, it has given valuable insights in optimizing thermal management and operational conditions for the 1 kg prototype system.

Acknowledgements

The funding for this study is provided by U.S. Department of Energy, under the contract DE-FC36-02AL67610 and the input of Dr. C. Read. The authors also acknowledge Mr. R. Brown for his valuable contribution in performing experimental work.

References

1. T. Kiyobayashi, S.S. Srinivasan, D. Sun and C.M. Jensen, J. Phys. Chem.A 107, 7671-7674 (2003).
2. G. Sandrock, K. Gross and G. Thomas, J. Alloys Comp. **339** 299-308 (2002).
3. K.J. Gross, E.H. Majzoub and S.W. Spangler, J. Alloys Comp. **356-357**, 423-428 (2003).
4. D.L. Anton, J. Alloys Comp. **356-357**, 400-404 (2003).
5. W. Luo and K.J. Gross, J. Alloys Comp. **385** 224-231 (2002).
6. I.A. El-Osery, Int. J. Hydrogen Energy, **8**, 191-198 (1983).
7. M.A. El-Osairy, I.A. El-Osery, A.M. Metwally and M.A. Hassan, J. Alloys Comp. **202**, 125-128(1993)
8. M.A. El-Gammal, I.A. El-Osery, A.M. Metwally and M.A. Hassan, Modeling, Measurement and Control, **46,** 35-44 (1994).
9. M.A. El-Osairy, I.A. El-Osery, A.M. Metwally and M.A. Hassan, Int. J. Hydrogen Energy, **18,** 517-524 (1993)
10. K.J. Gross, G.J. Thomas and C.M. Jensen, J. Alloys Comp. **330-332** 683-690 (2002).
11. G. Sandrock, K. Gross and G. Thomas, J. Alloys Comp. **339** 299-308 (2002).

Att.4 UTRC™ Sodium Alanate Kinetics 2

DLA

Kinetics Model Refinements

Dan Mosher
6/26/03

$NaAlH_4 \underset{r_2}{\overset{r_1}{\rightleftharpoons}} \frac{1}{3}Na_3AlH_6 + \frac{2}{3}Al + H_2 \underset{r_4}{\overset{r_3}{\rightleftharpoons}} NaH + Al + \frac{3}{2}H_2$

A number of refinements have been added to the kinetics model framework:

1. Check to make sure the composition variables are not outside the bounds of
$$0 \le C_i \le 1$$
2. Modify the reaction rate forms to allow different saturation hydrogen weight percentages at different temperatures.

1 Maintaining consistent values of the compositions, C_i ← Mole fractions?

1.1 Comment on Model Aspect which Keeps Consistent values of C_i

What is it in the modeling framework that maintains consistent values for the compositions? The consistency requirements are

$$0 \le C_i \le 1$$

and

Equation 1
$$\sum_{i=1}^{3} C_i = 1.$$

$C_1 \rightarrow NaH + Al + \frac{3}{2}H_2$
$C_2 \rightarrow \frac{1}{3}Na_3AlH_6 + \frac{2}{3}Al + H_2$
$C_3 \rightarrow NaAlH_4$
$dC_1 = dC_{NaH}$
$dC_2 = 3\,dC_{Na_3AlH_6}$
$dC_3 = dC_{NaAlH_4}$

For reaction 2 involving the hydriding of NaH (in the original model form with no saturation levels), we have

Equation 2
$$\left(\frac{dC_2}{dt}\right)_{r2} \propto (C_1)^{\chi_2}$$

Mol eqv NaH of $NaAlH_4$ $= C_{eqv} = C_{NaAlH_4} + 3C_{Na_3AlH_6} + C_{NaH}$
$C_i = \frac{C_{NaH}}{C_{eqv}}$ + C_{NaAlH_4}
$C_2 = \frac{C_{Na_3AlH_6}}{C_{eqv}}$
$C_3 = \frac{C_{NaAlH_4}}{C_{eqv}}$

This produces a C_2 that will reach a limit as $C_1 \rightarrow 0$, but it does not ensure that $0 \le C_2 \le 1$. However, the relationship which balances the product formation rate with the reactant consumption rate,

Equation 3
$$\left(\frac{dC_1}{dt}\right)_{r2} = -\left(\frac{dC_2}{dt}\right)_{r2}$$

when integrated over a small time step, will produce

$$(\Delta C_1)_{r2} = -(\Delta C_2)_{r2}$$

In this case,

$$(\Delta C_1 + \Delta C_2)_{r2} = (-\Delta C_2 + \Delta C_2)_{r2} = 0$$

If we consider pressure regime three where both reactions 2 and 4 are active, we will also have

$$(\Delta C_2 + \Delta C_3)_{r4} = 0$$

If we add these two equations,

Equation 4
$$(\Delta C_1 + \Delta C_2)_{r2} + (\Delta C_2 + \Delta C_3)_{r4} = 0$$

Since the model framework specifies that for pressure regime 3,

$$(\Delta C_1)_{total} = (\Delta C_1)_{r2}$$
$$(\Delta C_2)_{total} = (\Delta C_2)_{r2} + (\Delta C_2)_{r4}$$
$$(\Delta C_3)_{total} = (\Delta C_3)_{r4}$$

Equation 4 becomes

$$(\Delta C_1 + \Delta C_2 + \Delta C_3)_{total} = 0$$

or

$$C_1 + C_2 + C_3 = \text{constant}$$

If we start with values which sum to 1, then Equation 1 will be satisfied for all time.

Figure 1 demonstrates that this indeed does occur during the simultations even with the potential errors associated with numerical integration. The sum of C's is 1.000000 +/- 8e-7.

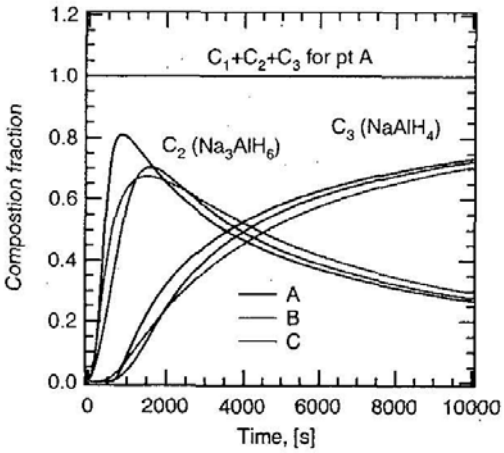

Figure 1: Composition results for four hole configuration.

1.2 Potential Issue with Numerical Integration which Should Be Corrected

With numerical integration, finite time steps are used. In this case, it is conceivable that the value of a reactant would not hit exactly 0 but could overshoot and become negative. An important influence of this is the value of the exponent χ on the composition variable. For the specific reaction of Equation 2 with $\chi_2 = 1$, if $C_1 < 0$ then $dC_2/dt < 0$ and by Equation 3, $dC_1/dt > 0$ which will self correct the value of C_1 toward 0. However, if $\chi_2 = 2$, the square of a negative number is a positive number, so that C_1 will become more negative in a run away numerical effect where C_1 becomes substantially less than 0 and C_2 becomes substantially greater than 1. As discussed above,

$$(\Delta C_1 + \Delta C_2)_{r2} = 0$$

would still apply but the individual values of C_1 and C_2 will diverge and be meaningless. Even though a value of $\chi = 2$ has been used in ABAQUS simulations, this problem has not been observed probably because the reaction rates slow down adequately as $C_1 \rightarrow 0$ so that the finite time steps do not produce an overshoot.

Nevertheless, modifications should be added to the coding to make sure that all of the compositions stay within the physical bounds of 0 and 1. One approach is to simply check the values of the compositions and if they are starting to deviate, to set them equal to 0 or 1 as appropriate. For the particular reaction, it also might be necessary to adjust the conjugate variable in the reaction to avoid any drifting of the composition sum. Another approach is to modify the coding used to represent Equation 2 as

$$\left(\frac{dC_2}{dt}\right)_{r2} \propto sign(C_1)*[abs(C_1)]^{\chi_2}$$

This has two advantages. First, the self correcting nature is preserved even if $\chi = 2$. Second, there will not be computation errors if C_1 is negative and the exponent is non-integer. Another, perhaps perferrable approach is to have

$$\left(\frac{dC_2}{dt}\right)_{r2} \propto [C_1]^{\chi_2} \text{ if } C_1 \geq 0$$

$$\left(\frac{dC_2}{dt}\right)_{r2} = 0 \text{ if } C_1 < 0$$

This essentially stops the hydriding reaction when the reactant concentration become slightly negative.

2 Modeling of Saturation Weight Percentages Which Vary with Temperature

2.1 Introduction

As shown in Figure 2, the saturation weight fraction absorbed can vary significantly with temperature. The value of 90 C is 0.02 and that for 100 C is 0.027. In the present modeling structure, the hydrogen weight fraction stored in the material is calculated from the composition variables as

Equation 5
$$w = \nu * (0.0187 * C_2 + 0.056 * C_3)$$

The variable ν represents the nonideal capacity. As a first attempt to fit the data in Figure 2, this variable was made temperature dependent,

Equation 6
$$w = \nu(T) * (0.0187 * C_2 + 0.056 * C_3)$$

and the comparison with data in Figure 2 is reasonably good at longer times. The complexities of the incubation period where not modeled and therefore the short time comparison is not good.

This approach is adequate to match the constant temperature data, but it will have unrealistic behavior when temperature is changing. As an example, if at 10,000 s, the temperature is changed from 90 to 100 C, the weight fraction will jump instantaneously from 0.02 to 0.027 which would not occur physically. Additional experiments in which the temperature is changed will be conducted to examine this effect.

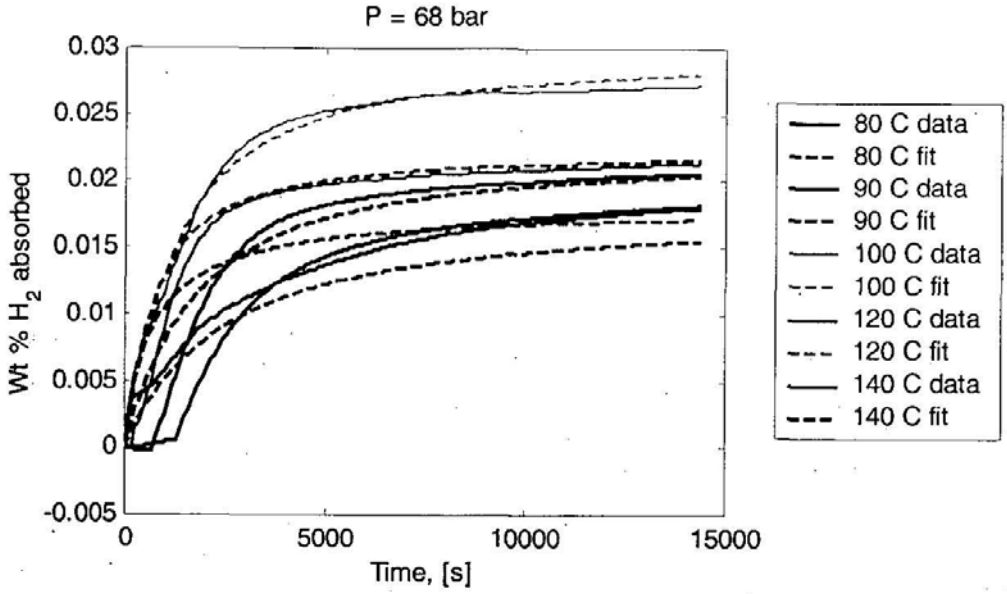

Figure 2: Absorption data for 6% TiCl3 with fit to constant temperature model.

2.2 Saturation Form for Single Composition, C_1

The framework modifications to allow for saturation weight fraction differences for arbitrary temperature histories are discussed next. One modeling approach is to have

$$\left(\frac{dC_2}{dt}\right)_{r2} \propto \left(C_1 - C_1^{sat}(T)\right)^{\chi_2}$$

which should be represented in the coding as

Equation 7
$$\left(\frac{dC_2}{dt}\right)_{r2} \propto \left[C_1 - C_1^{sat}(T)\right]^{\chi_2} \text{ if } C_1 - C_1^{sat}(T) \geq 0$$

Equation 8
$$\left(\frac{dC_2}{dt}\right)_{r2} = 0 \text{ if } C_1 - C_1^{sat}(T) < 0$$

The value of this saturation C_1 is calcuated by considering the resulting long-time composition,

$$C_1 = C_1^{sat}, \quad C_2 = 0, \quad C_3 = 1 - C_1^{sat}$$

and substituting these values into a modified version of Equation 5 where the obsolete factor of ν has been removed,

Equation 9
$$w = 0.0187 * C_2 + 0.056 * C_3$$

This results in a saturation value for the weight fraction under an isothermal temperature history of

$$w_{iso}^{sat} = 0.056 * \left(1 - C_1^{sat}\right)$$

or

Equation 10

$$C_1^{sat}(T) = 1 - \frac{w_{iso}^{sat}(T)}{0.056}$$

The parameter $w_{iso}^{sat}(T)$ represents the saturation level at long times for the absorbed weight fraction of hydrogen under an isothermal temperature history.

Because reaction 2 is a hydriding reaction, it can only proceed in the direction where C_2 is being produced and therefore we must have $C_1 > C_1^{sat}$. If not, then Equation 8 applies.

The equation for the second hydriding reaction would not necessarily need to be altered with a saturation level for the reactant,

$$\left(\frac{dC_3}{dt}\right)_{r4} \propto (C_2)^{\chi_4}.$$

To illustrate this with an example, consider if $w_{iso}^{sat} = 0.020$ and so $C_1^{sat} = 0.643$. If we start off with $C_1 = 1, \quad C_2 = 0, \quad C_3 = 0$, then after a long amount of hydriding, we would obtain $C_1 = 0.643, \quad C_2 = 0, \quad C_3 = 0.357$.
then we will obtain the desired value of

$$w = 0.0187 * 0 + 0.056 * 0.357 = 0.020$$

This approach appears to give reasonble physical behavior when changing temperatures for C_1^{sat} increasing with time. If for example, we hydride at 90 C for 10,000 s and then increase the temperature to 100 C, the value of C_1^{sat} will decrease and reaction 2 will become active again. This will produce a gradual change in w rather than the step change of Equation 6. Whether this rate of change matches experiment is another question which needs to be addressed with additional experiments.

2.3 Saturation Form for Two Compositions, C_1 and C_2

If we are not able to match experiments (or if we just prefer the approach below with more adjustable parameters), a possible modification is to have a saturation level of C_2^{sat} for reaction 4

Equation 11

$$\left(\frac{dC_3}{dt}\right)_{r4} \propto \left[C_2 - C_2^{sat}(T)\right]^{\chi_4} \text{ if } C_2 - C_2^{sat}(T) \geq 0$$

Equation 12

$$\left(\frac{dC_3}{dt}\right)_{r4} = 0 \text{ if } C_2 - C_2^{sat}(T) < 0$$

and to choose values of C_1^{sat} and C_2^{sat} from w_{iso}^{sat} so that they are consistent with the final capacity. For this, after long times of hydriding in pressure regime 3 at a certain temperature T,

$$C_1 = C_1^{sat}(T), \quad C_2 = C_2^{sat}(T), \quad C_3 = 1 - C_1^{sat}(T) - C_2^{sat}(T)$$

Applying Equation 9,

Equation 13

$$w_{iso}^{sat}(T) = 0.0187 * C_2^{sat}(T) + 0.056 * \left(1 - C_1^{sat}(T) - C_2^{sat}(T)\right)$$

There are two unknowns and one equation, so we cannot uniquely determine C_1^{sat} and C_2^{sat}. An assumption on their relationship to each other or additional data is required to proceed. If we relate the two saturation values by (an alternate relation given in Equation 17 below was used ultimately in the coding implementation)

$$R^{sat} = \frac{C_2^{sat}(T)}{C_1^{sat}(T)},$$

assuming that R^{sat} does not depend on temperature, then

Equation 14 $$C_2^{sat}(T) = R^{sat} * C_1^{sat}(T)$$

and from Equation 13,

$$w_{iso}^{sat}(T) = 0.0187 * R^{sat} * C_1^{sat}(T) + 0.056 * \left(1 - C_1^{sat}(T) - R^{sat} * C_1^{sat}(T)\right)$$

Solving for C_1^{sat},

$$w_{iso}^{sat} = C_1^{sat} * \left(0.0187 * R^{sat} + 0.056 * (-1 - R^{sat})\right) + 0.056$$

$$w_{iso}^{sat} - 0.056 = C_1^{sat} * \left(R^{sat} * (0.0187 - 0.056) - 0.056\right)$$

$$C_1^{sat} = \frac{w_{iso}^{sat} - 0.056}{R^{sat} * (0.0187 - 0.056) - 0.056}$$

and multiplying numerator and denominator by –1,

Equation 15 $$C_1^{sat} = \frac{0.056 - w_{iso}^{sat}}{0.056 + R^{sat} * (0.056 - 0.0187)}$$

And putting the temperature dependencies back in,

Equation 16 $$C_1^{sat}(T) = \frac{0.056 - w_{iso}^{sat}(T)}{0.056 + R^{sat} * (0.056 - 0.0187)}$$

As a check, if we only have C_1^{sat}, so that $R^{sat} = 0$, then

$$C_1^{sat} = \frac{0.056 - w_{iso}^{sat}}{0.056} = 1 - \frac{w_{iso}^{sat}}{0.056}$$

which agrees with Equation 10.

The parameter R^{sat} is an additional model parameter that can be adjusted to give the best match of all the data. In particular, it is expected that the data from temperature change tests will be the most useful in determining a representative value of R^{sat}. Also, it was noted in parameter fits that the value of R^{sat} produced an inflection of the curve in some circumstances.

Returning to Equation 13 and solving for $C_2^{sat}(T)$,

$$w_{iso}^{sat}(T) = (0.0187 - 0.056) * C_2^{sat}(T) + 0.056 * \left(1 - C_1^{sat}(T)\right)$$

$$(0.0187 - 0.056) * C_2^{sat}(T) = w_{iso}^{sat}(T) - 0.056 * \left(1 - C_1^{sat}(T)\right)$$

$$C_2^{sat}(T) = \frac{w_{iso}^{sat}(T) - 0.056*\left(1 - C_1^{sat}(T)\right)}{(0.0187 - 0.056)}$$

$$C_2^{sat}(T) = \frac{0.056*\left(1 - C_1^{sat}(T)\right) - w_{iso}^{sat}(T)}{(0.056 - 0.0187)}$$

If we hydride at 100 C to achieve the greatest capacity and then increase to 120 C, we would not expect the saturation weight fraction to drop to the lower level of a constant 120 C history. Experiments need to examine this. If experiments do find that the saturation weight fraction does not change after the temperature change from 100 to 120 C, then this will be consistent with the model described above. To step through examination of the model, when the temperature is increased from 100 to 120 C, the value of $w_{iso}^{sat}(T)$ will drop. The values of $C_1^{sat}(T)$ and $C_2^{sat}(T)$ determined from Equation 16 and Equation 14 will increase so that the arguments $\left(C_1 - C_1^{sat}\right)$ and $\left(C_2 - C_2^{sat}\right)$ will be less than zero and according to Equation 8 and Equation 12, the reaction rates will be zero as desired.

Physically, if $C_1^{sat}(T) = 1$, then both reactions r2 and r4 will be eliminated and the saturated weight fraction can be set as low as 0. However, setting $C_2^{sat}(T) = 1$ by itself will only restrict reaction r4. If $C_1^{sat}(T) \approx 0$ associated with large values of R^{sat}, then the minimum weight fraction stored will be 0.0187 and this will all occur during reaction r2 giving little opportunity for an inflected curve. Because of this, restrictions on valid values of R^{sat} and $w_{iso}^{sat}(T)$ would be needed.

Rather than attempt such restrictions, an alternate form relating $C_1^{sat}(T)$ and $C_2^{sat}(T)$ was developed. In order for $C_1^{sat}(T) \geq 0$,

$$0.056*\left(1 - C_1^{sat}(T)\right) \geq w_{iso}^{sat}(T)$$

$$C_1^{sat}(T) \leq 1 - \frac{w_{iso}^{sat}(T)}{0.056}$$

A convenient way to impose this restriction is to define

$$C_1^{sat,\max}(T) = 1 - \frac{w_{iso}^{sat}(T)}{0.056}$$

Then define a new independent parameter, r^{sat},

Equation 17

$$r^{sat} = \frac{C_1^{sat}(T)}{C_1^{sat,\max}(T)}$$

such that

$$C_1^{sat}(T) = r^{sat} * C_1^{sat,\max}(T)$$

or

Equation 18

$$C_1^{sat}(T) = r^{sat} * \left(1 - \frac{w_{iso}^{sat}(T)}{0.056}\right)$$

In this way, the restriction is easier to remember and enforce as $0 \le r^{sat} \le 1$. Note that the right hand factor in Equation 18 will also be between 0 and 1 for reasonable values of $w_{iso}^{sat}(T)$ so that after multiplying these two factors, we will have $0 \le C_1^{sat}(T) \le 1$. Once r^{sat} is chosen, compute $C_1^{sat}(T)$ from Equation 18 and compute $C_2^{sat}(T)$ from

$$C_2^{sat}(T) = \frac{0.056 * \left(1 - r^{sat} * \left(1 - \frac{w_{iso}^{sat}(T)}{0.056}\right)\right) - w_{iso}^{sat}(T)}{(0.056 - 0.0187)}$$

$$= \frac{\left(0.056 - r^{sat} * \left(0.056 - w_{iso}^{sat}(T)\right)\right) - w_{iso}^{sat}(T)}{(0.056 - 0.0187)}$$

$$= \frac{\left(1 - r^{sat}\right) * \left(0.056 - w_{iso}^{sat}(T)\right)}{(0.056 - 0.0187)}$$

or

Equation 19

$$C_2^{sat}(T) = \frac{\left(1 - r^{sat}\right) * \left(0.056 - w_{iso}^{sat}(T)\right)}{(0.056 - 0.0187)}$$

The form of Equation 19 shows that $C_2^{sat}(T)$ must go to zero as r^{sat} approaches 1 or $w_{iso}^{sat}(T)$ approaches 0.056. This is intuitive since the first condition is if all of the nonideal capacity is accounted for in $C_1^{sat}(T)$ and the latter is that the actual capacity equals the ideal level, i.e. no need for saturation compositions. An additional restriction is needed however, because it is possible for $C_2^{sat}(T)$ to become greater than 1 if $w_{iso}^{sat}(T)$ is less than 0.0187 and r^{sat} is 0 or nearly 0. To examine this second restriction,

$$C_2^{sat}(T) \le 1$$

$$\frac{\left(1 - r^{sat}\right) * \left(0.056 - w_{iso}^{sat}(T)\right)}{(0.056 - 0.0187)} \le 1$$

$$\left(1 - r^{sat}\right) * \left(0.056 - w_{iso}^{sat}(T)\right) \le (0.056 - 0.0187)$$

$$1 - r^{sat} \le \frac{(0.056 - 0.0187)}{\left(0.056 - w_{iso}^{sat}(T)\right)}$$

$$r^{sat} \ge 1 - \frac{0.056 - 0.0187}{0.056 - w_{iso}^{sat}(T)}$$

One characteristic of the model with both $C_1^{sat}(T)$ and $C_2^{sat}(T)$ is if we start out with an initial composition of $C_2 = 0$, the first hydriding reaction will need to proceed to the point were $C_2 > C_2^{sat}$ before reaction 4 will begin. Thus there will be a time lag between when some C_2 reactant is available and when reaction 4 becomes active. This may produce an inflection in the curve.

2.4 *Modified Form for All Pressure Regimes*

The previous examination has focused just on pressure regime 3 for which both reactions are proceeding in the hydriding direction. For reversible reactions, we would anticipate that the amount stored would need to equal the amount released, at least after steady state has been reached. Because the amount stored was limited by introducing saturation levels for C_1 and C_2, the amount released will already be limited and we do not need to change the form for the dehydriding reactions (although the parameters will need to be modified from previous estimates). Another way to consider whether to have saturation levels on the dehydriding reactions is to think that in the dehydriding direction, we want all of the reactants to be consumed so the compositions can return to the initial state of $C_1 = 1, \quad C_2 = 0, \quad C_3 = 0$. If we have saturation levels for C_2 or C_3, then the dehydriding rate will go to zero before the compositions drop to zero. Therefore, we do not want saturation values on the reactants for the dehydriding reactions.

In the current model framework, the composition at the start of hydriding test after complete dehydriding would be

$$C_1 = 1, \quad C_2 = 0, \quad C_3 = 0$$

and the composition at the start of dehydriding after complete hydriding at temperature T would be

$$C_1 = C_1^{sat}(T), \quad C_2 = C_2^{sat}(T), \quad C_3 = 1 - C_1^{sat}(T) - C_2^{sat}(T)$$

A sketch of the three pressure regimes is shown in Figure 3.

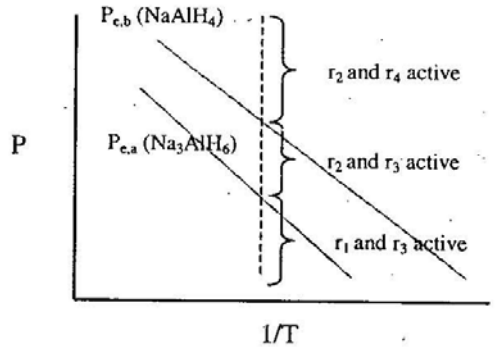

Figure 3: Reaction pressure regimes.

The complete model for all three pressure regimes will be,

Table 1: Complete listing of reaction rate equations.

Pressure regime 1 r1 and r3 active	If $C_2 \geq 0$, $\left(\frac{dC_1}{dt}\right)_{r1} = A_1 \exp\left(-\frac{E_1}{RT}\right) * \left(\frac{P_{e,1} - P}{P_{e,1}}\right) * (C_2)^{\chi_1}$ $\left(\frac{dC_2}{dt}\right)_{r1} = -\left(\frac{dC_1}{dt}\right)_{r1}$ If $C_3 \geq 0$, $\left(\frac{dC_2}{dt}\right)_{r3} = A_3 \exp\left(-\frac{E_3}{RT}\right) * \left(\frac{P_{e,3} - P}{P_{e,3}}\right) * (C_3)^{\chi_3}$ $\left(\frac{dC_3}{dt}\right)_{r3} = -\left(\frac{dC_2}{dt}\right)_{r3}$
Pressure regime 2 r2 and r3 active	If $C_1 - C_1^{sat}(T) \geq 0$, $\left(\frac{dC_2}{dt}\right)_{r2} = A_2 \exp\left(-\frac{E_2}{RT}\right) * \left(\frac{P - P_{e,2}}{P_{e,2}}\right) * \left(C_1 - C_1^{sat}(T)\right)^{\chi_2}$ $\left(\frac{dC_1}{dt}\right)_{r2} = -\left(\frac{dC_2}{dt}\right)_{r2}$ If $C_3 \geq 0$, $\left(\frac{dC_2}{dt}\right)_{r3} = A_3 \exp\left(-\frac{E_3}{RT}\right) * \left(\frac{P_{e,3} - P}{P_{e,3}}\right) * (C_3)^{\chi_3}$ $\left(\frac{dC_3}{dt}\right)_{r3} = -\left(\frac{dC_2}{dt}\right)_{r3}$
Pressure regime 3 r2 and r4 active	If $C_1 - C_1^{sat}(T) \geq 0$, $\left(\frac{dC_2}{dt}\right)_{r2} = A_2 \exp\left(-\frac{E_2}{RT}\right) * \left(\frac{P - P_{e,2}}{P_{e,2}}\right) * \left(C_1 - C_1^{sat}(T)\right)^{\chi_2}$ $\left(\frac{dC_1}{dt}\right)_{r2} = -\left(\frac{dC_2}{dt}\right)_{r2}$ If $C_2 - C_2^{sat}(T) \geq 0$, $\left(\frac{dC_3}{dt}\right)_{r4} = A_4 \exp\left(-\frac{E_4}{RT}\right) * \left(\frac{P - P_{e,4}}{P_{e,4}}\right) * \left(C_2 - C_2^{sat}(T)\right)^{\chi_4}$ $\left(\frac{dC_2}{dt}\right)_{r4} = -\left(\frac{dC_3}{dt}\right)_{r4}$

If the quantities stated in Table 1 which need to be ≥ 0 are actually < 0, then the associated reaction rate is set to 0.

For all three pressure regimes, the total rate of change for C_2 will be the sum for each of the two active reactions,

$$\left(\frac{dC_2}{dt}\right)_{total} = \left(\frac{dC_2}{dt}\right)_{\text{r1 or r2}} + \left(\frac{dC_2}{dt}\right)_{\text{r3 or r4}}$$

As present previously, the equilibrium pressure is

$$\ln(P_e) = \frac{\Delta H}{RT} - \frac{\Delta S}{R}$$

or

Equation 20

$$P_e(T) = \exp\left(\frac{\Delta H}{RT} - \frac{\Delta S}{R}\right).$$

3 Effect of Parameters on Curve Characteristics

Some parameter fitting and sensitivity studies were conducted with the initial relation of Equation 14 using R^{sat} for the saturation compositions. The value of R^{sat} influences the weight fraction level at which the inflection point occurs for the transition between the reactions. This is shown in Figure 4 through Figure 7 for the 100 C data. A slightly different set of parameters was used to fit the 120 C data shown in Figure 8 through Figure 11.

Using Equation 17 to choose different values of the saturation compositions, it seemed more difficult to produce the inflection point in the curves during parameter estimatation trials using MATLAB. There is no restriction in the new form that should make this happen, and it is likely that this was caused by having different values of the other model parameters that affect the relative rates etc. of the two hydriding reactions. A small amount of thought was invested into what conditions would lead to a more prominent inflection region, but this was shelved in the interest of completing the model and its application. For an inflection region to occur, one needs reaction 2 to slow down, to have reaction 4 become active, to have reaction 2 still proceed to produce more reactant for reaction 4 but to have reaction 4 accelerate in hydrogen production. It is still unclear what values of the parameters (or dependencies between them) will produce a pronounced inflection region.

The fit to experimental data using Equation 17 is shown in Figure 12 using the parameter values of Table 2. The value of r^{sat} was set equal to 1 for all temperatures, which in effect sets $C_2^{sat} = 0$ and would appear to eliminate the possibility of an inflection region. Other parameter combination are still possible to give a better match. Nevertheless, the results are reasonably good. The fit at 140 C is the poorest due to the large inflection region. The model was also fit to the desorption data shown in Figure 13. A different value for $C_1^{sat} = 0.5$ was used to best match the resulting capacities. We could argue that such flexibility in choosing C_1^{sat} is acceptable since we do not known the actual composition of the as received / milled material.

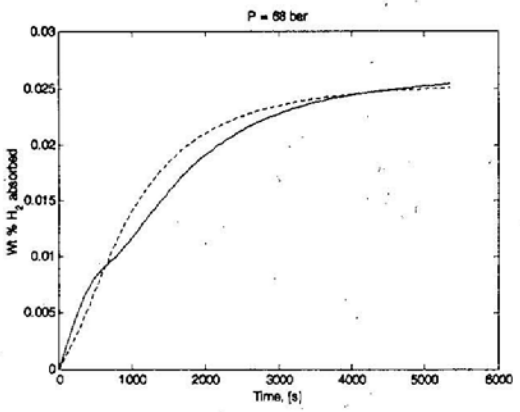

Figure 4: Data (solid) and model (dashed) for absoption at 100 C with $R^{sat} = 0$.

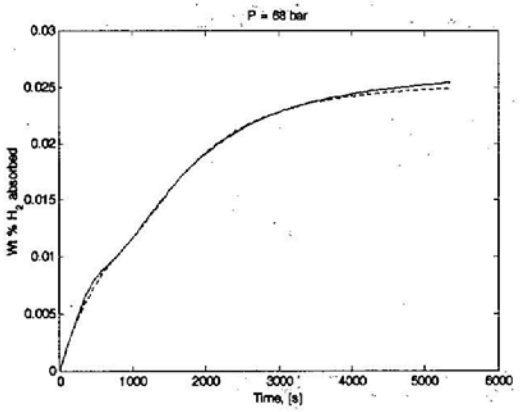

Figure 5: Data (solid) and model (dashed) for absoption at 100 C with $R^{sat} = 3$.

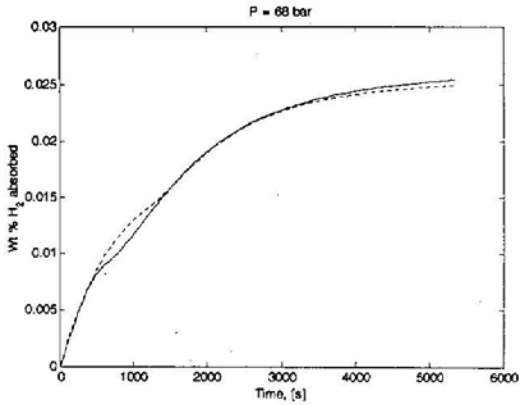

Figure 6: Data (solid) and model (dashed) for absoption at 100 C with $R^{sat} = 10$.

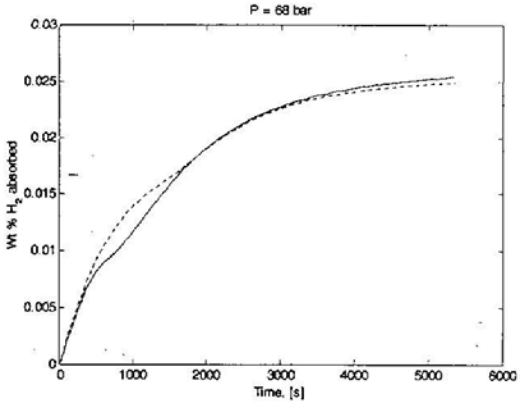

Figure 7: Data (solid) and model (dashed) for absoption at 100 C with $R^{sat} = 1000$.

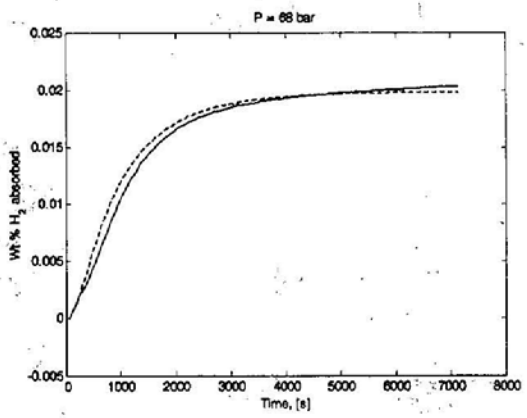

Figure 8: Data (solid) and model (dashed) for absoption at 120 C with $R^{sat} = 0$.

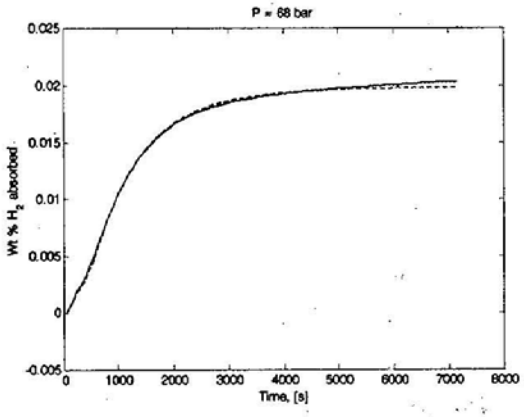

Figure 9: Data (solid) and model (dashed) for absoption at 120 C with $R^{sat} = 0.2$.

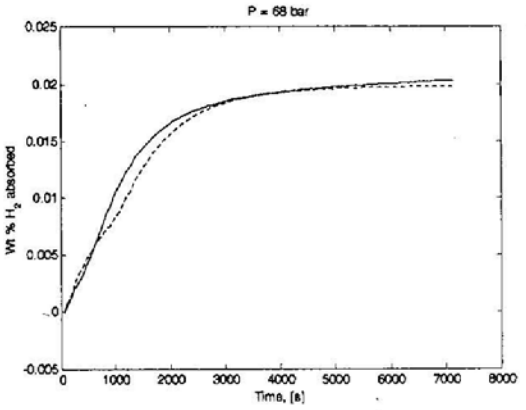

Figure 10: Data (solid) and model (dashed) for absoption at 120 C with $R^{sat} = 1$.

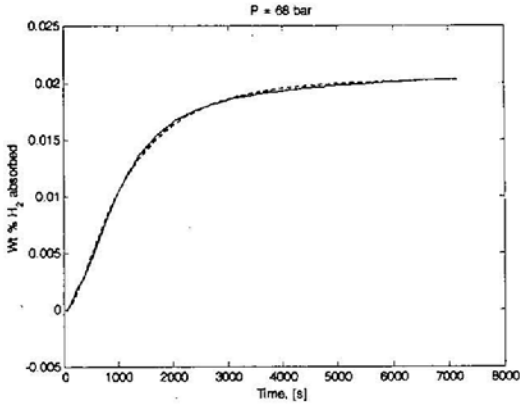

Figure 11: Data (solid) and model (dashed) for absoption at 120 C with $R^{sat} = 0$ with other parameter optimized (A_T reduced from 7.0e4 to 5.5e4, w_sat increased from 0.020 to 0.0205).

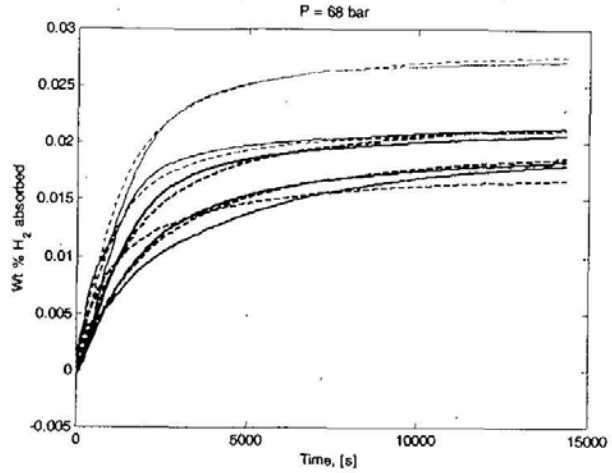

Figure 12: Absorption with starting C_1 = 1 and T dependent C_1_sat (r_sat(T) = 1 so C_2_sat = 0). The dashed lines are the model with red=80C; blue=90C; cyan=100C; green=120C; and magenta=140C.

Table 2: MATLAB coding giving model parameter values.

```
T_sat_C = [0    80    90    100   120   140   300 ];     % temperatures associated with w_iso
w_sat =  [0.021 0.021 0.023 0.029 0.022 0.018 0.018];   % saturation weight fractions at tempertures T_iso_C
r_sat =  [1     1     1     1.0   1     1     1   ];      % ratio of C_1_sat / C_1_sat_max
r_sat_threshold = 1 - (0.056 - 0.0187) ./ (0.056 - w_sat);  % restriction level for r_sat, 1 - (0.056 - 0.0187) / 0.056 = 0.333
r_sat = max(r_sat, r_sat_threshold);          % check for values of r_sat that will maintain C_2_sat < 1.
T_sat_K = T_sat_C + 273;

i_r = 1; % directional reaction 1, dehydriding of Na3AlH6 to NaH
      param(i_r,1) = -6150;     % A or delta H / R, slope in van't Hoff plot
      param(i_r,2) = 16.22;     % B or -delta S / R, intercept in van't Hoff plot
      param(i_r,3) = 6.0e12;    % A_T, leading coefficient in temperature factor, time unit of seconds
      param(i_r,4) = 110000;    % E, thermal activation energy, J / mol of H_2
      param(i_r,5) = 1.0;       % chi, exponent on reactant weight fraction
i_r = 2; % directional reaction 2, hydriding of NaH to Na3AlH6
      param(i_r,1) = -6150;     % A, not used, value for i_r = 1 used
      param(i_r,2) = 16.22;     % B, not used, value for i_r = 1 used
      param(i_r,3) = 1.5e5;     % A_T
      param(i_r,4) = 70000;     % E
      param(i_r,5) = 1.0;       % chi
i_r = 3; % directional reaction 3, dehydriding of NaAlH4 to Na3AlH6
      param(i_r,1) = -4475;     % A, used for r3 and r4
      param(i_r,2) = 14.83;     % B, used for r3 and r4 (14.83)
      param(i_r,3) = 4.0e12;    % A_T
      param(i_r,4) = 110000;    % E
      param(i_r,5) = 2.0;       % chi
i_r = 4; % directional reaction 4, hydriding of Na3AlH6 to NaAlH4
      param(i_r,1) = -4475;     % A, not used, value for i_r = 3 used
      param(i_r,2) = 14.83;     % B, not used, value for i_r = 3 used (14.83)
      param(i_r,3) = 1.0e8;     % A_T
      param(i_r,4) = 80000;     % E
      param(i_r,5) = 2;         % chi
```

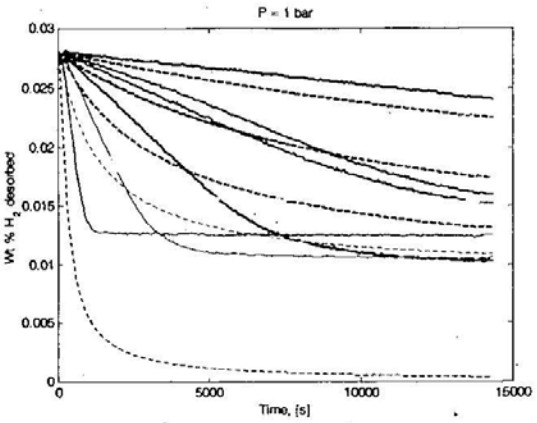

Figure 13: Desorption from as milled condition (assume C_1_sat = 0.5). Dashed lines are model. Temperatures are black=70C; red = 80 C (two experiments); blue=90C; cyan=100C; yellow=110C; green=120C;

Note that the equilibrium pressure for the lower van't Hoff line using a modified Equation 20 and parameters in Table 2 is

$$P_e(T) = \exp\left(\frac{A}{T} + B\right) = \exp\left(\frac{-6150}{T} + 16.22\right)$$

Solving for the transition temperature for the desorption pressure of 1 atm,

$$T = \frac{-6150}{\ln(P_e(T)) - 16.22} = \frac{-6150}{\ln(1\,\text{atm}) - 16.22} = 379\,\text{K} = 106\,\text{C}$$

Thus, we would expect significant differences in capacity for temperatures above 106 C versus those below it. This is reflected in the model predictions of Figure 13 (yellow and green lines) but not in the experimental data. In fact, after 8,000 s, the desorbed capacity at 90 C is greater than at 120 C. Additional experimentation and modeling is required to understand this effect.

The modifications to the kinetics model were made to the ABAQUS subroutines and check with a simple isothermal test problem. The user subroutine "powder_user2.for" was developed from the previous "powder_user.for" file based on additional modeling and parameter estimation in MATLAB. The implementation of changes required adding parameters to calculate saturation compositions and also the addition of these saturation levels to the hydriding reaction rate equations. Simple simulations were conducted in ABAQUS to verify that the implementation was accurate. These were nearly isothermal simulations of a cube 0.1m in size. A slight temperature difference was produced by imposing a convective boundary condition which was 1 degree C higher than the initial temperature to avoid numerical problems of taking to small of a time step in transient thermal analyses. Such a small time (100 s) is needed to integrate the reaction equations.

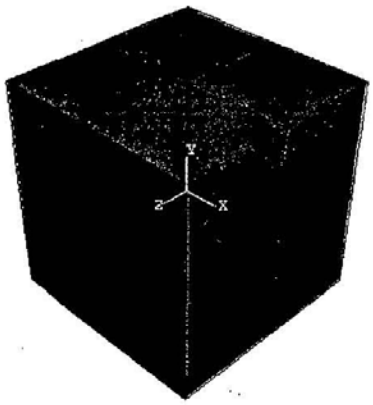

Figure 14: 0.1 meter cube used to test implementation of model in ABAQUS.

The results below are very similar to the comparison of data with the MATLAB implementation as expected. After these simulations were run, code was added to the user subroutine HETVAL to check whether the composition factors were positive. A simulation at 140 C was then rerun and the results did not changed at all. This is expected since the value of r_sat was 1 for all temperatures so that C_2_sat = 0 and therefore there would not be any negative composition factors for an isothermal history starting with C_1 = 1. Note that the checks for negative composition factors were in the MATLAB code used to fit the parameters. Therefore, though the code was modified, it is expected that the results for the other temperatures besides 140 C will also agree as in the figure.

The results in Figure 15 show good agreement with Figure 12 indicating the coding of equations including their integration is accurate, at least for these conditions.

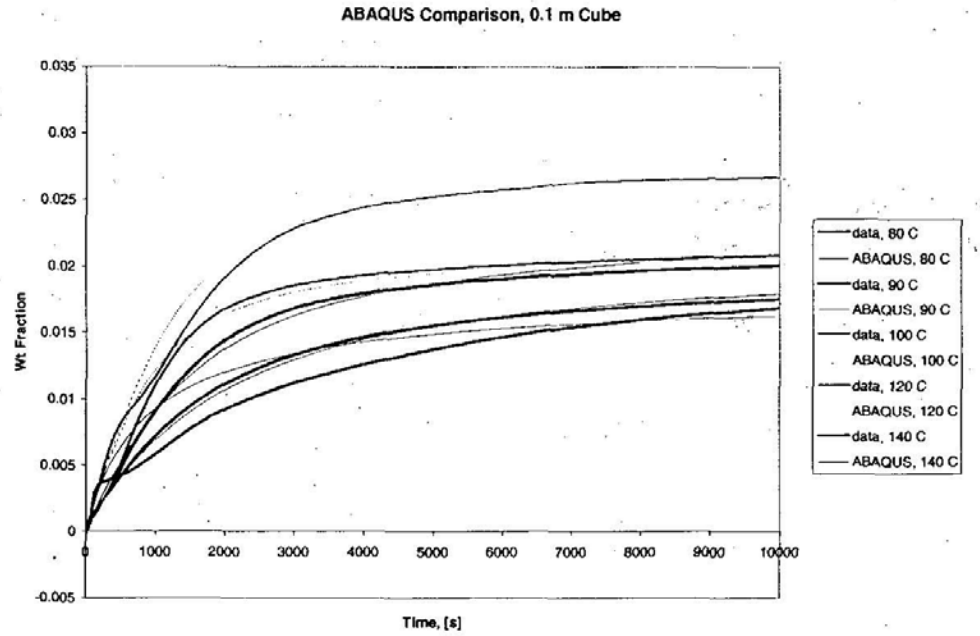

Figure 15: Results for absorption conditions.